Journal of Controlled Release 381 (2025) 113615

Contents lists available at ScienceDirect

Journal of Controlled Release

journal homepage: www.elsevier.com/locate/jconrel

Disulfiram-loaded electrospun fibers with antimicrobial and antitumoral properties for glioblastoma treatment

Iago Gonzalez-Prada [a], Arthur Barcelos Ribeiro [b], Marine Dion [b], Beatriz Magariños [c], Clémentine Lapoujade [b], Audrey Rousseau [b,d], Angel Concheiro [a], Emmanuel Garcion [b,e,f,*], Carmen Alvarez-Lorenzo [a,**]

[a] Departamento de Farmacología, Farmacia y Tecnología Farmacéutica, I+D Farma (GI-1645), Facultad de Farmacia, Instituto de Materiales (iMATUS) and Health Research Institute of Santiago de Compostela (IDIS), Universidade de Santiago de Compostela, Spain
[b] Inserm UMR 1307, CNRS UMR 6075, Université de Nantes, CRCI2NA, Université d'Angers, 49000 Angers, France
[c] Departamento de Microbiología y Parasitología, Facultad de Biología-CIBUS and Aquatic One Health Research Center (iARCUS), Universidade de Santiago de Compostela, Spain
[d] Department of Pathology, University Hospital of Angers, F-49000 Angers, France
[e] PACEM (Plateforme d'Analyse Cellulaire et Moléculaire), Université d'Angers, SFR 4208, F-49000 Angers, France
[f] PRIMEX (Plateforme de Radiobiologie et d'Imageries Expérimentales), Université d'Angers, SFR 4208, F-49000 Angers, France

ARTICLE INFO

Keywords:
Glioblastoma
Disulfiram
Silk fibroin
Cyclodextrin
Copper
Electrospinning

ABSTRACT

Glioblastoma (GB) is a malignant brain tumor with low survival rates and a high recurrence ratio due to limited therapeutic arsenal. The repurposed drug disulfiram (DSF), approved for alcoholism treatment, shows promising anticancer and antimicrobial activity, but its poor biopharmaceutical profile hinders its clinical use. This work aimed to develop DSF-loaded silk fibroin (SF) electrospun fibers for controlled release in the postsurgical resection cavity. Incorporating hydroxypropyl-β-cyclodextrin (HPβCD), which formed inclusion complexes with DSF, enhanced drug release rate and antimicrobial activity (>3 logCFUs reduction) against *Staphylococcus aureus* and *Pseudomonas aeruginosa*. Addition of $CuCl_2$ enabled in situ formation of $Cu(DDC)_2$ complexes, further boosting antimicrobial and in vitro antitumoral effects of the nanofibers (≤ 500 nm) while maintaining adequate mechanical properties. Selective toxicity of DSF and DSF-loaded fibers against glioblastoma cells, while sparing against astrocytes, highlights the potential of the nanofibers for targeted brain cancer therapy. Increased potency of DSF at low concentrations when combined with SF fibers, HPβCD and copper was remarkable. Thus, DSF delivery and bioavailability can be significantly optimized through electrospun nanofibers, which may also allow for more precise dosing. Combination with radiotherapy was also explored to assess the translational potential of DSF as part of a combination therapy regimen for glioblastoma. In vivo studies in a rat model simulating GB surgery confirmed the safety of selected formulations in healthy brain tissue. However, findings suggest that DSF-loaded fibers alone may be insufficient for complete tumor eradication, indicating the need for combination with existing therapies to target residual tumor cells effectively.

1. Introduction

Glioblastoma (GB) is a highly aggressive and lethal brain tumor characterized by a poor prognosis owing to its location, fast progression, and noteworthy invasive nature throughout the Central Nervous System [1]. Globally, approximately 49% of all primary brain tumors are GBs and its incidence tends to increase with age, mainly affecting adults between 45 and 75 years of age. The current standard treatment for GB consists of surgical resection to reduce the tumor mass followed by radiation and chemotherapy with temozolomide [2]. Different chemotherapeutic agents (i.e., lomustine, carmustine, nimustine and, and regorafenib), immunotherapy (i.e., bevaciuzumab), and anti-mitotic therapies that generates Tumor Treating Fields (TTFields) (i.e. Optune™, previously known as the NovoTTF-100 A System™) are

* Corresponding author at: Inserm UMR 1307, CNRS UMR 6075, Université de Nantes, CRCI2NA, Université d'Angers, 49000 Angers, France.
** Corresponding author at: Departamento de Farmacología, Farmacia y Tecnología Farmacéutica, Facultad de Farmacia, Universidade de Santiago de Compostela, 15782 Santiago de Compostela, Spain.
E-mail addresses: emmanuel.garcion@univ-angers.fr (E. Garcion), carmen.alvarez.lorenzo@usc.es (C. Alvarez-Lorenzo).

https://doi.org/10.1016/j.jconrel.2025.113615
Received 31 October 2024; Received in revised form 2 February 2025; Accepted 7 March 2025
Available online 12 March 2025

explored as new treatment options. Despite the numerous investigations on GB diagnosis and treatment, the overall 5-year survival remains at 9.8% due to multiple factors, including cellular heterogeneity, protection by the blood-brain barrier, dissemination capacity through neighboring tumor structures, and intrinsic resistance of the mesenchymal glioblastoma stem cells, also known as tumor-initiating cells [3]. Additionally, therapeutic alternatives usually come with high associated costs, present a poor treatment compliance, and have risks of neurologic deficits and severe side effects like suppression of bone marrow, hepatotoxicity, nephrotoxicity, necrosis, neurotoxicity, hematologic toxicity, and skin toxicity [4]. The intracranial local implant Gliadel® (carmustine wafer) approved by FDA for recurrent GB has demonstrated an improvement in median of overall survival and progression-free survival of 2 months, supposing a quality-adjusted life years (QALY) of only 0.107 (5.6 weeks) [5] while it has remarkable limitations associated to the difficulty in handling, interferences with imaging (MRI), lack of wound healing, high probably of meningitis and oedema apparition, and short time therapy (6–8 weeks) leading a progressive clinical use reduction [6].

Considering the high attrition rates, substantial costs, and slow progress of the discovery and development of new therapeutic strategies, drug repurposing has emerged as an attractive alternative. Basically, drug repurposing (also referred as drug repositioning, reprofiling or re-tasking) is an approach for identifying new uses for already approved or investigational drugs that are outside the scope of the original clinical indication [7]. Disulfiram is a good illustration of a drug repositioning opportunity that might offer an effective treatment for GB therapy [8,9].

Disulfiram (DSF) was approved by the Food and Drug Administration (FDA) in 1951 to treat chronic alcohol dependency (Antabuse®) by acting as an inhibitor on aldehyde dehydrogenase isoform-1A3 (ALDH1A3) [9]. Several preclinical and clinical studies have suggested that DSF could have potent anticancer properties against several types of cancer, including GB. Although the mechanisms behind the cytotoxic effect of DSF on cancer cells remain not completely elucidated, the results obtained so far revealed an important versatile anticancer activity. As a divalent metal ion chelator, DFS can strongly chelate Cu(II) highly expressed in cancer cells to form a copper-DSF complex (Cu(II) bis (diethyldithiocarbamate); $Cu(DDC)_2$) that downregulates several copper-dependent signaling pathways responsible for DNA reparation and promotes reactive oxygen species (ROS) toxicity, resulting in a reduction of cancer cell viability by apoptosis induction [10–12]. This mechanism allows a targeted antitumoral activity, since cancer cells exhibit higher levels of intracellular Cu (2–3-fold) compared with healthy cells (e.g., the content in Cu of normal brain is 5.37 μg/g whilst malignant glioma tissue has 22.69 μg/g) [13]. Additionally, DSF may act as a proteasome inhibitor [14]. More specifically, DSF alone or in combination with Cu(II) targets nuclear protein localization protein 4 (NPL4), thus leading to their aggregation. Consequently, the p97-dependent protein turnover pathway is inactivated, followed by the induction of the unfolded protein response (UPR) causing an accumulation of misfolded proteins, endoplasmic reticulum stress and apoptosis [15–17]. $Cu(DCC)_2$ inhibits permanently the activity of P-gp efflux pump and its expression levels [18,19]. In parallel, DSF may be useful against drug-resistant cancer cells since it has demonstrated an inhibitory activity over the activation of the nuclear factor-κB (NF-κB) [20]. Also, DSF has cytotoxic activity over cancer stem cells that overexpresses several markers and transcription factors including aldehyde dehydrogenases (ALDHs), Sox2, Nanog and Oct3/4, which are targeted and inhibited by DSF [16]. DSF might also suppress cancer progression by inhibiting the proteolytic matrix metalloproteinases-2 [21], which regulates the migration and invasion features of cancer cells. Concomitant administration of DSF and temozolomide can cause synergistic effects, decreasing cell proliferation and self-renewal and successfully overcoming drug resistance [16]. Overall, DSF can be considered a multifunctional chemotherapeutic agent with a pronounced capacity to regulate cancer cell growth, differentiation, spontaneous metastasis, and drug resistance, all of which are vital to the development and progression of cancer.

Apart from this important anticancer activity, DSF also presents anti-inflammatory and antibacterial properties. More specifically, DSF has revealed a strong activity against Gram-positive bacteria *Staphylococcus aureus (*MIC ranging from 0.37 to 64 μg/mL) and a slight activity against the Gram-negative bacteria *Pseudomonas aeruginosa (*MIC around 512 μg/mL) [22]. These properties may be particularly useful to prevent and control infections after surgical tumor resections in patients with GB [23]. Collectively, the antitumor, antibacterial, and anti-inflammatory activities of DSF, make this drug one of the strongest ones to be repositioned to clinical GB treatment. However, DSF is a biopharmaceutical classification system (BCS) class II drug (i.e., low solubility and high permeability) and its clinical applications in GB treatment are limited by its lipophilicity (logP 4.16), poor water solubility (0.2 mg/mL), physiological instability, and short plasma half-life (ca. 7 h) [24,25]. Consequently, systemic administration demands high doses of free DSF (ca. 500–1000 mg once daily) or in combination with temozolomide (ca. 500 mg once daily) [17] to guarantee the desired therapeutic effect, but this causes marked hepatotoxicity, neurotoxicity, and low patient compliance, which urges the development of local delivery devices [26]. Moreover, the extremely low solubility of $Cu(DDC)_2$ (0.1–0.2 μg/mL, 50-fold more hydrophobic respect to DSF) and readily formation of aggregates makes practically impossible its systemic administration [18,27].

The development of post-operative electrospun mats as locally implantable treatment for GB is particularly appealing compared to conventional chemotherapy. The insertion of electrospun mats inside the tumor resection cavity would be negligibly invasive since surgery is part of the standard of care of patients with GB. Electrospun fiber mats are highly versatile regarding drug (including DSF) entrapment efficiency and physical properties, provide high surface-to-volume ratio and porosity to promote drug release, and can be easily adapted to any space [28,29]. Thereby, tumor-implanted electrospun mats avoid the blood-brain barrier crossing, increase cancer-targeted drug bioavailability, reduce systemic exposition, can mimic the native GB extracellular matrix, and allow the concomitant administration of drugs with synergistic activities [29–31].

Considering all these aspects, this work was aimed to obtain an electrospun scaffold that can provide antitumoral and antimicrobial effects for recurrent GB patients, using the repurposed drug DSF and its complex with copper, $Cu(DCC)_2$. Silk fibroin (SF) was selected as main structural polymer of the fibers, HPβCD as encapsulating agent, and $CuCl_2$ as an adjuvant molecule. SF transition from α-helix to β-sheet conformation communicates robust mechanical strength and toughness to a variety of scaffolds [32]. Notably, SF is a promising candidate for clinical use after GB resection surgery, since it displays intrinsic bioactivities such as anti-inflammatory, hemostatic, neuroprotective, restorative neurological, and regenerative nerve process activities [33–35]. By forming inclusion complexes, HPβCD imparts stability and notably increases DSF apparent solubility [36]. HPβCD also displays neuroprotective and anticancer effects by forming complexes with fatty acids and cholesterol, mitigates the inflammatory effect response of immune cells, and reduces the production of interleukins (IL-10) and cytokines (TNF-α) [37]. Indeed, HPβCD has been approved as an orphan drug for the treatment of focal segment glomerulosis and the Niemann pick disease type C [38]. Combination of CDs and electrospinnable polymers may result in important synergies such as enhanced tensile strength, facilitated wetting of the mats, favored erosion or dissolution of the fibers, and most importantly a high encapsulation efficiency [39–41].

Some ongoing GB clinical trials involve the administration of DSF and Cu(II) in separate and by different vias [19,42] and result in the non-targeted exposition of the patient to high blood levels of both components (with toxic effects) for short periods of time (short half-life). As a relevant innovative approach, the developed electrospun fibers could

function as local depots of both DSF and Cu(II) facilitating in situ formation of DSF-copper complex where it is needed. The DSF-loaded electrospun mats were produced by electrospinning and characterized using a wide range of analytical techniques including FTIR and SEM, contact angle measurements, and mechanical tests. After the structural characterization, hemocompatibility, and antimicrobial performance against relevant bacteria were investigated. Selective antitumoral activity against GB was assessed using glioblastoma cell lines from murine (GL261) and human (U-87MG) origin, human glioblastoma astrocytoma cells (U-251MG) and also non-tumor fibroblasts (NIH-3T3) and non-tumor primary astrocytes. The use of Cu(II) in combination with DSF could be an attractive approach to increase the anticancer activity and reduce the amount of drug, leveraging the chelator activity of DSF for several organometallics, namely zinc, iron, and copper. $CuCl_2$ was chosen as a source of Cu(II) since both elements (Cu and Cl) are naturally present in human body [43]. Likewise, Cu is involved in different normal homeostasis brain and neuronal process, including DNA regulation, cofactor of myriad enzymatic reactions, redox regulation, mitochondrial respiration, antioxidant defense, neural firing, cellular metabolism, and synaptic plasticity [44,45]. Thus, the lack of this ion promotes the apparition of severe neurodegenerative disease (i.e., amyotrophic lateral sclerosis, Alzheimer, Huntington, and Parkinson's disease). Moreover, brain has considerable tolerance at great amounts of copper (up to 125 μg/g dry weight) owing to the presence of astrocytes that recollect and store the copper to protect and supply the nervous system [46,47]. Furthermore, Cu(II) could be an useful organometallic for scaffold due to the antimicrobial properties, decreasing the occurrence of infection and promoting vessel formation through the secretion of VEGF, angiogenin (hAmg), and fibroblast grow factor 1 (FGF1), IL-1, and IL-8 [48,49]. The addition of Cu(II) in the electrospun fibers may allow increasing its intratumor concentration to easily generate high levels of $Cu(DDC)_2$, improving the effectiveness of the therapy and reducing inter-cancer and inter-patient differences, offering an alternative to intravenously injected DSF-loaded targeted nanoparticles [50]. A prospective, exploratory study aimed at understanding the impact and behavior of DSF fibers in the brain, both in naïve animals and in tumor-bearing models, was carried out.

2. Materials and methods

2.1. Materials

Fresh silk fibroin (SF) solution 7% (*w/v*) was supplied by IMIDA (Murcia, Spain). It was stored at −80 °C for 4 h and then freeze-dried for 48 h (LyoQuest, Telstar; Barcelona, Spain). 1,1,1,3,3,3-Hexafluoro-2-propanol (HFIP) was purchased from Acros (Waltham, MA, USA). Hydroxypropyl-β-cyclodextrin (HPβCD) was obtained from Roquette (Lestrem, France). Disulfiram (tetraethylthiuram disulfide), sodium diethyldithiocarbamate (DDC), Triton X-100, sodium dodecyl sulfate 95%, Dulbecco's Modified Eagle's Medium - high glucose (D6429), Dulbecco's Phosphate Buffered Saline (D8537), Trypsin-EDTA solution (T3929), Antibiotic Antimycotic Solution (A5955), Fetal Bovine Serum (CVFSVF00–01), copper(II) chloride dihydrate (C3279), resazurin sodium salt (R7017), Giemsa stain (GS500), and dimethyl sulfoxide (DMSO, 41639) were purchased from Sigma-Aldrich (Steinheim, Germany). L-glutamine were provided by BioWhittaker (Verviers, Belgium). Dimethylformamide (DMF) and copper chloride (II) anhydride were provided by Thermo Fisher Scientific (Waltham, MA, USA). Phosphate-buffered saline (PBS) pH 7.4, 6.5, and 5.5 media were prepared as indicated in the European Pharmacopoeia 6th edition. For pH 7.4, 8 g/L NaCl, 2.38 g/L Na_2HPO_4 and 0.19 g/L KH_2PO_4 were mixed in ultrapure water. Acetonitrile and ethanol were provided by VWR Chemicals (Leuven, Belgium). Ultrapure water (resistivity>18.2 MΩ cm; Milli-Q®, Millipore Ibérica, Madrid, Spain) was obtained by reverse osmosis.

$Cu(DDC)_2$ was synthesized as previously reported [51] by mixing $CuCl_2$ (0.04 g in 500 mL water) and DDC (0.134 g in 500 mL water) under gentle agitation overnight. The obtained solid brown precipitate was filtered, washed with ultrapure water and recrystallized with pure ethanol (> 99%) to eliminate impurities and unreacted products. The final product was dried under vacuum and subsequently analyzed by FTIR (**Fig. S1**) to confirm $Cu(DDC)_2$ complex formation.

2.2. Preparation of polymeric solution and electrospinning

Freeze-dried SF 12.5% (*w/v*) was dissolved in HFIP at 40 °C under gentle agitation for 48 h and the solution was transferred to a syringe for the electrospinning. Disulfiram 0.5% and 5.0% (w/v) was added to some solutions and kept under stirring overnight before the electrospinning.

SF 12.5% (*w/v*) HPβCD 10% (*w/v*) fibers were prepared in two steps. Firstly, 1 g of freeze-dried SF was dissolved in 4 mL of HFIP at 40 °C under gentle agitation for 12 h. In parallel, 0.8 g of HPβCD was dissolved in 4 mL of HFIP at room temperature under strong agitation overnight. Then, both solutions were mixed under gentle agitation overnight. Finally, to prepare SF 12.5% (*w/v*) HPβCD 10% (w/v) disulfiram 0.5–5.0% (w/v) fibers disulfiram was added to the HPβCD solution to prepare the inclusion complex.

SF 6% (w/v) $CuCl_2$ 0.045% (w/v) fibers were prepared in two steps. Firstly, 0.5 g of freeze-dried SF was dissolved in 3.6 mL of HFIP at 40 °C under gentle agitation for 5 h. Meanwhile, 0.004 g of $CuCl_2$ was dissolved in 0.4 mL of DMF by strong agitation using a vortex for 1 min, after that, the same volume of HFIP was added. Then, both solutions were mixed under strong agitation at 40 °C drop by drop. To prepare the fibers with DSF at 0.5% and 5%, 0.05 g and 0.5 g were added to the previously homogeneous solution and mixed under gentle agitation overnight.

SF 5% (*w/v*) HPβCD 0.51–2.6% (w/v) $CuCl_2$ 0.045% (w/v) fibers were prepared in three steps. Firstly, 0.4 g of freeze-dried SF was dissolved in 2.6 mL of HFIP at 40 °C under gentle agitation for 5 h. Secondly, 0.004 g of $CuCl_2$ was dissolved in 0.4 mL of DMF by strong agitation using a vortex for 1 min, after that, the same volume of HFIP was added. Then, both solutions were mixed under strong agitation at 40 °C drop by drop. Thirdly, HPβCD (0.51 g or 2.6 g) was dissolved in 1 mL of HFIP at room temperature for 2 h. DSF (0.05 g or 0.5 g) was added to the HPβCD solution at room temperature and kept under gentle agitation during 8 h. Finaly, this solution was incorporated to the aforementioned SF-$CuCl_2$ solution and kept under gentle agitation overnight.

A climate-controlled Yflow® Professional Electrospinning Machine (Yflow® S.D., Málaga, Spain) was used for fibers preparation. A series of experiments were carried out varying the electrospinning parameters to optimize the process. The applied voltages ranged between 10 and 15 kV, the collection distance was set at 15–25 cm, and the feeding rate was 1.0–2.0 mL/h. Composition and electrospinning condition for each fiber are summarized in Table 1 and **Table S1**, respectively.

Table 1
Composition of the electrospun fibers expressed per gram of solid material.

Fiber type (*w/v*)	SF (mg)	HPβCD (mg)	DSF (mg)	Cu (mg)
SF (12.5%)	1000			
SF (12.5%) DSF (0.5%)	962		38	
SF (12.5%) DSF (5%)	714		286	
SF (12.5%) HPβCD (10%)	556		444	
SF (12.5%) HPβCD (2.6%) DSF (0.5%)	801	167	32	
SF (12.5%) HPβCD (10%) DSF (5%)	455	364	182	
SF (6%) $CuCl_2$ (0.045%)	993			7
SF (6%) DSF (0.1%) $CuCl_2$ (0.045%)	976		16	3.4
SF (6%) DSF (0.5%) $CuCl_2$ (0.045%)	917		76	3.2
SF (5%) HPβCD (0.51%) DSF (0.1%) $CuCl_2$ (0.045%)	884	90	18	3.7
SF (5%) HPβCD (2.6%) DSF (0.5%) $CuCl_2$ (0.045%)	614	319	61	2.6

2.3. Fibers characterization

Electrospun mats were coated by sputtering gold under argon (Sputter Coater (Au) - QUORUM Q150T-S) and observed using a ZEISS FESEM ULTRA Plus (Carl Zeiss, Oberkochen, Germany). The average diameter was determined using the ImageJ image analysis software (**Fig. S2**).

Mechanical properties were analyzed, in triplicate, using a TA.XT plus Texture Analyzer (Stable Micro Systems, Surrey, UK) equipped with a 30 Kgf (~294 N) load cell under a crosshead speed of 10 mm/min. The fibers were cut as square pieces of 2.0 cm × 2.0 cm. The Young's modulus was determined as the slope of the linear (elastic) region of the stress-strain curve. Tensile strength and elongation at break (%) were also calculated.

The hydrophobicity of the fibers was determined from the contact angle of water, formamide and 1-bromonafthalene using an OCA 15 Plus equipment (Dataphysics Instruments, Germany), plugged with a video-camera for image acquisition and later data analysis. Pieces of the fibers (1 cm × 6 cm) were glued to a glass slide with double-sided tape, and 6 to 10 measurements were made at room temperature (23 ± 2 °C) following a previously described protocol [41].

2.4. In vitro release study

SF mats containing disulfiram (1cm^2 square, average weight 0.035 g) were immersed in 2–10 mL of PBS (pH 7.4, 6.5, and 5.5) and incubated at 100 rpm and 37 °C in a continuous shaker. At predetermined time points, 200 μL of solution was removed, filtered (Scharlau® Syringe Filter, 0.22 μm 13 mm HPPTFE), and replaced with 200 μL of fresh PBS. The release profile was determined using HPLC (AS-4140 autosampler, PU-4180 pump, LC-NetII/ADC interface box, CO-4060 column oven, MD-4010 photodiode array detector, JASCO, Tokyo, Japan) fitted with a C18 column (Waters Symmetry C18, 5 μm, 4.6 × 250 mm) and operated with ChromNAV software v.2. The mobile phase was acetonitrile:water 70:30 (*v*/v) over 9 min. The sample injection volume was 10 μL and the eluent was pumped at flow rate of 1 mL/min for 9 min. DSF was detected at 3.43 min at a wavelength of 217 nm (**Fig. S3**) and $Cu(DCC)_2$ was detected at 6.74 min at a wavelength of 432 nm (**Fig. S4**). The detection limit (LOD) and the quantification limit (LOQ) were determined to be 0.622 ppm and 1.882 ppm for DSF, and 0.088 ppm and 0.266 ppm for $Cu(DCC)_2$, respectively (**Figs. S5 and S6**). The experiments were conducted in triplicate.

2.5. Blood compatibility

A 2.5% (*v*/v) blood solution stock was prepared by diluting 5 mL of total blood provided by Galician Transfusion Center (ADOS) previously anticoagulated with EDTA in 200 mL of PBS (pH 7.4). SF mats (1 cm^2 square pieces) were immersed in 5 mL of 2.5% (*v*/v) blood solution stock and incubated at 37 °C for 2 h under shaking. After that, the falcon tubes were centrifuged at 2400 *g* for 10 min. Then, 150 μL of supernatant was taken and placed in a 96 well plate. The hemolytic activity was calculated as a function of the released hemoglobin which was measured by recording absorbance of the supernatant (Abs_{sample}) using a UV–visible microplate reader (Fluostar Optima, BMG Labtech, Germany) at 510 nm. Triton X-100 4% (v/v) solution was used as the positive control (PC) (100% lysis) and PBS (7.4) was added to blood stock solution and used as the negative control (NC). The hemolysis percentage was calculated using Eq. (1):

$$\%Hemolysis = \frac{(Abs_{sample} - Abs_{NC})}{(Abs_{PC} - Abs_{NC})} \times 100 \quad (1)$$

2.6. Antimicrobial activity

2.6.1. Bacterial strains and growth media

The antibacterial activity of the different SF electrospun mats were evaluated against *Staphylococcus aureus* (ATCC 25923) and *Pseudomonas aeruginosa* (CECT 110). All microbial strains were preserved at −80 °C in cryovial and 30% glycerol and subcultured in trypticase soy agar (TSA) for *S. aureus* and Luria-Bertani's lysogenic agar (LB) for *P. aeruginosa* at 37 °C during 12 h before testing.

2.6.2. Antimicrobial test

The method was based on the American Society for Testing and Materials (ASTM E-2149) standard. Briefly, the bacteria inoculum was prepared by aseptically transferring isolated colonies to 40 mL of trypticase soy agar (TSA) nutrient broth for *S. aureus* and 40 mL of Luria-Bertani's lysogenic broth (LB) for *P. aeruginosa*, and then incubated for 12 h at 37 °C. After that, the inoculum was diluted at $OD_{620\ nm}$ of 0.04 ± 0.02 (corresponding to a concentration of ~1 × 10^8 cells/mL; [41]). Electrospun mat pieces (1 cm^2; ≈ 0.35 mg) were sterilized under UV light for 15 min per side, placed in a sterile 24 well-plate with 2 mL microorganism suspension and incubated for 24 h at 37 °C under slightly stirring (100 rpm). After that contact time, 100 μL of microorganism suspension of each sample was taken and added to 900 μL of PBS in an Eppendorf. Then, seven dilution factors 1:9 (*v*/v) were performed. For each dilution factor, 10 μL were spread on nutrient agar plates and incubated at 37 °C for 24 h. Then, the viable colonies were counted, and results were expressed in log CFU/mL using Eq. (2) [52]:

$$\frac{CFU}{mL} = \frac{N}{SV \times Dilution} \quad (2)$$

Where N is the number of CFU and SV is the volume of the sample in mL. The logarithmic reduction values were calculated according to Eq. (3) [52]:

$$logreduction = logCFU/mL_{control} - logCFU/mL_{sample} \quad (3)$$

where the controls were SF 12.5% and SF 12.5% HPβCD 10% (without DSF) fibers, and the designation "sample" refers to fibers containing disulfiram.

Four replicate experiments were performed for each sample, testing two replicates in different weeks, and the growth reduction was evaluated according to the Japanese Industrial Standard, as no antimicrobial activity (<0.5 log reduction), slight antimicrobial activity (0.5 to 1 log reduction), significant antimicrobial activity (1 to 3 log reduction) and strong antimicrobial activity (>3 log reduction) [53].

2.7. In vitro test

2.7.1. Cells and culture conditions

Non-tumor murine fibroblasts NIH-3T3 (CRL-1658™) and human glioblastoma cell line U-87MG (HTB-14 ™) were acquired from ATCC (Rockville, Maryland, USA). The murine glioblastoma cell line GL261 (RRID: CVCL_Y003) was kindly provided by Corinne Griguer and G. Yancey Gillespie of the University of Alabama at Birmingham, AL, USA. Human glioblastoma astrocytoma cell line U-251MG was a gift from C. Griguer and originally obtained from Dr. D.D. Bigner (Duke University, Durham, NC, USA). Cell lines were cultivated in Dulbecco's Modified Eagle's Medium - high glucose, supplemented with 10% fetal bovine serum and 1% antibiotic antimycotic solution. Cultures were maintained at 37 °C in a 5% CO_2 environment. Purified newborn mice primary astrocytes were obtained by the mechanical dissociation method from cultures of cerebral cortex as originally described [54]. The cells were grown at 37 °C/5% CO_2 in DMEM with glucose and L-glutamine containing 10% fetal bovine serum and 1% antibiotic antimycotic solution.

2.7.2. Cytotoxicity assessment of DSF

The assessment of DSF cytotoxic potential, in association with 1 μM of Cu^{2+}, was conducted using the resazurin colorimetric assay based on the reduction of the oxidized blue dye by living cells into a pink, fluorescent resorufin product. For experimentation, 2.5×10^4 (24 h) and 1.5×10^4 cells (48 h) were seeded into 24-well plates and incubated at 37 °C in a 5% CO_2 atmosphere. DSF was initially dissolved in DMSO and subsequently diluted in complete medium. Concentrations ranging from 0.03 to 1 μM were tested. Control wells, consisting of negative (untreated), solvent (DMSO - 0.0297%), copper (1 μM), and positive (DMSO - 25%) controls, were included. Following a 24 or 48-h incubation period with DSF at 37 °C in a 5% CO_2 environment, the culture medium was aspirated to remove treatments before exposure to resazurin (44 μM). Microplates were then incubated at 37 °C in a 5% CO_2 environment for 2 h. Fluorescence intensity was measured using a multi-plate reader (CLARIOstar® Plus) with excitation at 544 nm (545–20) and emission at 590 nm (600–40). Non-linear regression analysis was performed using GraphPad Prism to determine the sample concentration that inhibits 50% of cell viability (IC_{50}, half maximal inhibitory concentration).

2.7.3. Clonogenic assay

The antiproliferative potential of DSF in combination with 1 μM of Cu^{2+} was assessed using the clonogenic efficiency assay [55]. The exposure time and treatment concentrations were determined based on prior cytotoxicity assays. U-87MG, U-251MG, and GL261 cell suspensions were seeded into 6-well plates at a density of 300 cells per well. After allowing the cells to adhere during a 2-h incubation at 36.5 °C in 5% CO_2, the cell lines were treated with varying concentrations of DSF (0.025–0.30 μM) in association with 1 μM of Cu^{2+}. Following 24 h of treatment, the culture medium was removed, and the cells were washed with PBS to eliminate any remaining treatment. The cells were then incubated to allow for at least six cell division cycles. After this incubation period, the colonies were washed with PBS, fixed with PFA 4%, and stained with Giemsa stain for 20 min. Finally, the colonies were counted, and the survival fraction was calculated according to the formula provided by Franken et al. [55].

2.7.4. Cytotoxicity assessment of DSF combined with beam radiation

The evaluation of cytotoxic potential of DSF-fibers in combination with irradiation was also performed using the resazurin colorimetric assay. For this experimentation, the test was conducted on the mouse primary astrocytes, and on cell lines NIH-3T3 and GL261, seeded at a density of 1×10^4 cells/mL in 24-well plates. After 24 h of incubation at 37 °C in a 5% CO_2 atmosphere the cells were exposed to different concentrations of DSF (dissolved in DMSO and diluted in complete medium) ranging from 0.03 μM to 0.12 μM. Control wells, consisting of negative (untreated), solvent (DMSO - 0.0297%), copper (1 μM), and positive (DMSO - 25%) controls, were included. Following a 24-h incubation period with DSF at 37 °C in a 5% CO_2 environment, the culture medium was aspirated to remove treatments and replaced by fresh medium before an exposition to irradiation at 16GY (CP-160 cabinet X-ray system Faxitron, Edimex, Le Plessis Grammoire, Angers, France). After 48-h incubation, the cells were exposed to resazurin (44 μM), and microplates were incubated at 37 °C in a 5% CO_2 environment for 2 h. Fluorescence intensity was measured using a multi-plate reader (CLARIOstar® Plus) with excitation at 544 nm (545–20) and emission at 590 nm (600–40). Non-linear regression analysis was performed using GraphPad Prism to determine the sample concentration that inhibits 50% of cell viability (IC_{50}, half maximal inhibitory concentration).

2.7.5. Cytotoxicity assessment of DSF nanofibers

Cells were seeded at a density of 5×10^4 cells/mL in 24-well plates and incubated for 24 h at 37 °C in a 5% CO_2 atmosphere. Subsequently, the cells were exposed to electrospun fiber pieces (4.91 mm^2, ≈ 0.20 mg) immerged in 1 mL of complete medium and further incubated at 37 °C for 24 h. Control wells encompassed negative controls (untreated), SF 12.5%, SF 6% $CuCl_2$ 0.045%, SF 6% HPβCD 2.6% $CuCl_2$ 0.045% solutions, and positive (DMSO - 25%) controls. Test wells contained SF 12.5% DSF 5% fibers, SF 12.5% DSF 0.5% fibers, SF 12.5% HPßCD 2.6% DSF 0.5% fibers, SF 6% DSF 0.5% $CuCl_2$ 0.045% fibers, SF 6% DSF 0.1% $CuCl_2$ 0.045% fibers, SF 5% HPßCD 2.6% DSF 0.5% $CuCl_2$ 0.045% fibers, and SF 5% HPßCD 0.51% DSF 0.1% $CuCl_2$ 0.045% fibers. Following a 24-h incubation at 37 °C, the culture medium was aspirated to remove treatments before exposure to resazurin (44 μM). Microplates were then incubated at 37 °C in a 5% CO_2 environment for 2 h. Fluorescence intensity was measured using a multi-plate reader (CLARIOstar® Plus) with excitation at 544 nm (545–20) and emission at 590 nm (600–40). Non-linear regression analysis was performed using GraphPad Prism to determine the effect of fibers on cell viability.

2.8. Evaluation of the toxicity of fibers in vivo

2.8.1. Animals

15 Fisher female rats aged 9–11 weeks were obtained from Janvier Labs (Le Genest-Saint-Isle, France). The protocol was approved by the Ethical Committee for Animal Experimentation of Pays de la Loire region, France (authorization number APAFIS # 43915–2020032620074335). A minimum acclimatization period of one week was conducted before beginning the experiments. Rats were provided with ad libitum access to tap water and food. In this work, each rat represents an independent experimental unit.

2.8.2. Implantation of fibers

Two types of fibers were chosen to evaluate the toxicity in a complete normal brain: SF 12.5% HPßCD 2.6% DSF 0.5% fibers, and SF 5% HPßCD 2.6% DSF 0.5% $CuCl_2$ 0.045% fibers. These fibers were first cut using a biopsy punch of 3 mm in diameter and sterilized under UV light for 15 min per side. Fisher rats were divided into three groups: a control group with 5 rats which undergo the surgery without receiving the fiber, a first treated group of 4 rats that received the fiber without cupper (one rat did not survive during the procedure) and a second treated group of 5 rats that received the fiber with cupper. Rats were anesthetized intraperitoneally with ketamine (0.8 mL/kg) and xylazine (0.62 mL/kg) and positioned in a Kopf stereotaxic instrument. A 10 mm incision was made along the midline to expose the surface of the skull. Subsequently, rats' skulls were pierced with a burr (Microtorque II) following these coordinates from the bregma (=0 mm): lateral: −2.9 mm, anteroposterior: +1 mm. A hole approximately 3 mm in diameter was created to allow a biopsy punch to access the cortex. The brain tissue was carefully cut and removed using vacuum suction, forming a cavity about 2 mm deep. One piece of fiber was gently placed into the cavity, the skull was then closed using bone wax and the wound was sutured. The rats were kept under observation for a week before euthanasia.

Surgical stereotaxis with dedicated stereotaxic frames was carried out as previously reported on an validated model, ensuring low variability in residual disease after resection [32]. Similar methods have been reported by other authors in mice [56,57] and rats [58]. All technical procedures, including anesthesia and surgery, were performed and supervised by trained specialists. The creation of a moderate-volume cavity (approximately 9.5 μL) had no impact on the animal's comfort, behavior and quality of life.

2.8.3. Histology and anatomocytopathology

After euthanasia, the brains were collected and subsequently fixed in 4% formaldehyde for around 10 days, followed by paraffin embedding. Afterward, 5 μm thick sections were obtained using an HM340E Microm Microtech microtome (France) and stained with hematoxylin and eosin (HE) for analysis. Several histopathological parameters were considered to assess the impact of fiber implantation on the brain such as multinucleated giant cells, acute inflammatory cells, necrosis, chronic inflammatory cells, neoangiogenesis, hemorrhage, hemosiderin deposition, and mineralization. Histopathological analyses were carried

out at the Department of Cellular and Tissue Pathology of the University Hospital Center of Angers (CHU-Angers, France). The slides were scanned using an Aperio system.

2.9. In vivo evaluation of the effect of DSF fibers on residual GB cells growth

To evaluate the specific effects of DSF fibers on tumor development from residual glioblastoma cells present within resection cavity margins, a brain resection cavity was created (P: +1.3 mm; L: −3.0 mm (right from the bregma); D: ~ −2.5 mm from the cortex surface) in 10 Fisher female rats aged 9–11 weeks obtained from Janvier Labs. The protocol was approved by the Ethical Committee for Animal Experimentation of Pays de la Loire region, France (authorization number APAFIS # 43915–2,020,032,620,074,335). DSF fibers (3-mm diameter) were carefully implanted in the hollow of this cavity. The animal groups were as follows: 3 animals for cavity control, 3 for DSF fibers, and 4 for DSF + Cu^{2+} fibers. Then, 1×10^3 RG2 cells (ATCC, [D74] CRL-2433 ™) were injected at 1 mm posterior from the edge of the resection (stereotactic coordinates: P: +1.3, L: −4, D: −1.5 mm from the surface of the brain). Excess blood was removed with sterile gauze, the cavities were closed with non-absorbable bone wax and the wound was sutured. This method allowed for the precise implantation of a determined amount of tumor cells in resection margins adjacent to an accessible cortex resection cavity [32].

2.10. Statistical analysis

Statistical analysis was performed using SPSS v.26.0 (IBM Co., Armonk, NY, USA). All results were expressed as mean ± standard deviation. Statistical analyses of the antimicrobial and antioxidant results (one-way ANOVA) were conducted, followed by the post hoc Tukey HSD multiple comparison test. Previously statistical analysis normality of all variables was evaluated using Kolmogorov-Smirnov test for groups ($n \geq 50$) and Shapiro–Wilk test for groups ($n \leq 50$). A confidence interval was used at least 95%, to define statistical significance (* $p < 0.05$, ** $p < 0.005$, *** $p < 0.001$ and **** $p < 0.0001$).

3. Results and discussion

3.1. Fibers preparation and morphological and mechanical analysis

Preliminary studies were carried out to evaluate the effect of SF concentration (10% to 20% (*w/v*) range) on the spinnability and morphology of electrospun fibers. All SF solutions tested were electrospun under the same experimental conditions, but only SF 12.5% solution maintained an adequate Taylor cone for hours showing good properties for spinnability. SF fibers displayed continuous, smooth, homogeneous fibers without noticeable beads (Fig. 1A). Size distributions of fiber diameters are collected in **Fig. S2**.

Once SF concentration was fixed, the effect of HPβCD concentration was investigated. For the aim of this work, DSF concentration was chosen to be 0.5 or 5.0% (*w/v*). To encapsulate a large amount of drug (5.0% (w/v)), 20% (w/v) of HPβCD may be required if a 1:1 complex is considered [36,59]. Unfortunately, the properties of SF solution were notably altered. The Taylor cone was unstable even many different parameters were attempted to be adjusted, and many drops were collected in the aluminum foil. Thus, HPβCD concentration had to be reduced to 10% (*w/v*) to obtain homogeneous electrospun fibers of SF 12.5% (w/v) HPβCD 10% (w/v) using the same parameters as for 12.5% (w/v) SF fibers (Fig. 1B).

Incorporation of disulfiram did not alter the electrospinnability, and electrospun fibers were obtained for SF 12.5% (*w/v*) DSF 0.5–5.0% (w/v) fibers, although the fiber diameter distribution was wider in the case of disulfiram 0.5% (Fig. 1C**, Fig. S2C**) compared to 5.0% (Fig. 1D). The drug was successfully encapsulated, and no disulfiram crystals were found lengthwise the fibers in the SEM images either.

As expected, the inclusion complex between HPβCD (10% w/v) and disulfiram (5% w/v) did not change the electrospun parameters (Table 1). Overall, all fiber compositions provided continuous, smooth, homogeneous fibers without noticeable beads (Fig. 1 ***E-F***). SF 12.5% (*w/v*) fibers had a diameter of 1.51 ± 0.42 μm whereas SF 12.5% (*w/v*) HPβCD 10% (w/v) electrospun fiber diameter was 1.79 ± 0.37 μm (Fig. 1N). Therefore, no statistically significant differences were observed. The addition of disulfiram at 5% (*w/v*) to SF 12.5% (w/v) caused a minor decrease in the diameter of the fibers, 1.11 ± 0.22 μm. Differently, the addition of disulfiram to HPβCD solutions did not decrease the size of the fibers, reaching 1.57 ± 0.3 μm.

To reinforce the antitumor effect, $CuCl_2$ was added to the solutions to be electrospun. The incorporation of $CuCl_2$ at 0.045% (*w/v*) in the SF 6.0% (w/v) solution was challenging due to its insolubility in solvents commonly used for dissolving and stabilizing silk fibroin in β-sheet conformation (i.e., formic acid and HFIP). DMF was selected as the most suitable solvent owing to its capacity to readily dissolve $CuCl_2$ at 0.45% (*w/v*) without inducing precipitation of SF at 4.0% (w/v) in HFIP at ratio of 10% (*v/v*). Indeed, homogeneous, continuous, smooth, and without beads fibers was obtained from this polymeric solution (Fig. 1G). The concentration of SF had to be decreased from 12.5% (*w/v*) to 6.0% (w/v) to avoid precipitation in the presence of $CuCl_2$ at 0.045% (*w/v*). This phenomenon was due to the interaction of Cu(II) ions with SF amino acid residues of histidine and tryptophan through coordination with both N and O atoms. Some authors reported that Cu(II) can chelate SF chains forming cross-linking networks. Moreover, metal ions change the conformation from helical conformation to β-sheet in several proteins including SF [60].

The reduction in SF concentration decreased the diameter of the fibers (reaching nano scale) and improved the morphology changing form ribbon structure to cylinder structure. Thus, SF 6% (*w/v*) $CuCl_2$ 0.045% (w/v) fibers were homogeneous, continuous, smooth and without undesired beads (Fig. 1H). The incorporation of HPβCD at 2.6% (w/v) and DSF at different concentrations 0.1–0.5% (w/v) did not cause further changes (Fig. 1I,J,K). Nevertheless, SF 6% (w/v) HPβCD at 2.6% (w/v) $CuCl_2$ 0.045% (w/v) showed a slightly increase in the size fiber 0.63 ± 0.21 μm, if compared with SF 6% (w/v) $CuCl_2$ 0.045% (w/v) displaying a 0.41 ± 0.16 μm. As expected, SF 6% (w/v) DSF 0.1% (w/v) $CuCl_2$ 0.045% produced thinner fibers (0.25 ± 0.08 μm) than SF 6% (w/v) DSF 0.5% (w/v) $CuCl_2$ 0.045% (0.44 ± 0.20 μm). Smaller fibers were obtained with a further decrease in SF concentration to 5% (w/v) and incorporating HPβCD 0.51% (w/v) DSF 0.1% (w/v) $CuCl_2$ 0.045% (w/v) or HPβCD at 2.6% (w/v) DSF 0.5% (w/v) $CuCl_2$ 0.045% (w/v). Both fibers displayed diameters of 0.17 ± 0.10 μm and 0.19 ± 0.10 μm respectively, maintaining the same characteristics and morphology as the other SF mats (Fig. 1L,M**)**.

3.2. Mechanical, spectroscopical and hydrophobic properties of the fibers

SF 12.5% fibers showed high Young's modulus and tensile strength (Table 2**)** due to its high content in SF in β-sheet conformation [61]. Addition of $CuCl_2$ notably reinforced the mechanical properties of the fibers despite the decrease in SF concentration. Differently, incorporation of HPβCD and DSF caused a weakening in the mechanical properties due to their intercalation between SF beta chains, suggesting an intermolecular disruption. Nevertheless, even the weaker mats had mechanical properties similarly to those of pure PCL electrospun mats [41] and ensured correct application in the resection cavity.

The presence of SF, HPβCD and disulfiram in the fibers was checked by comparing the FTIR spectra (**Fig. S7)**. The characteristic peaks of SF appeared at 1242 cm^{-1} (C—N stretching vibration of amide III),1526 cm^{-1} (N—H bending vibration and C—N stretching vibration of amide II), and 1631 cm^{-1} (C—O stretching vibration of amide 1) assigned with numbers 3,5 and 6 in Fig. S7). These three bands indicated that SF was in β-sheet conformation (silk II) [29]. Typical bands of HPβCD at 1027 cm^{-}

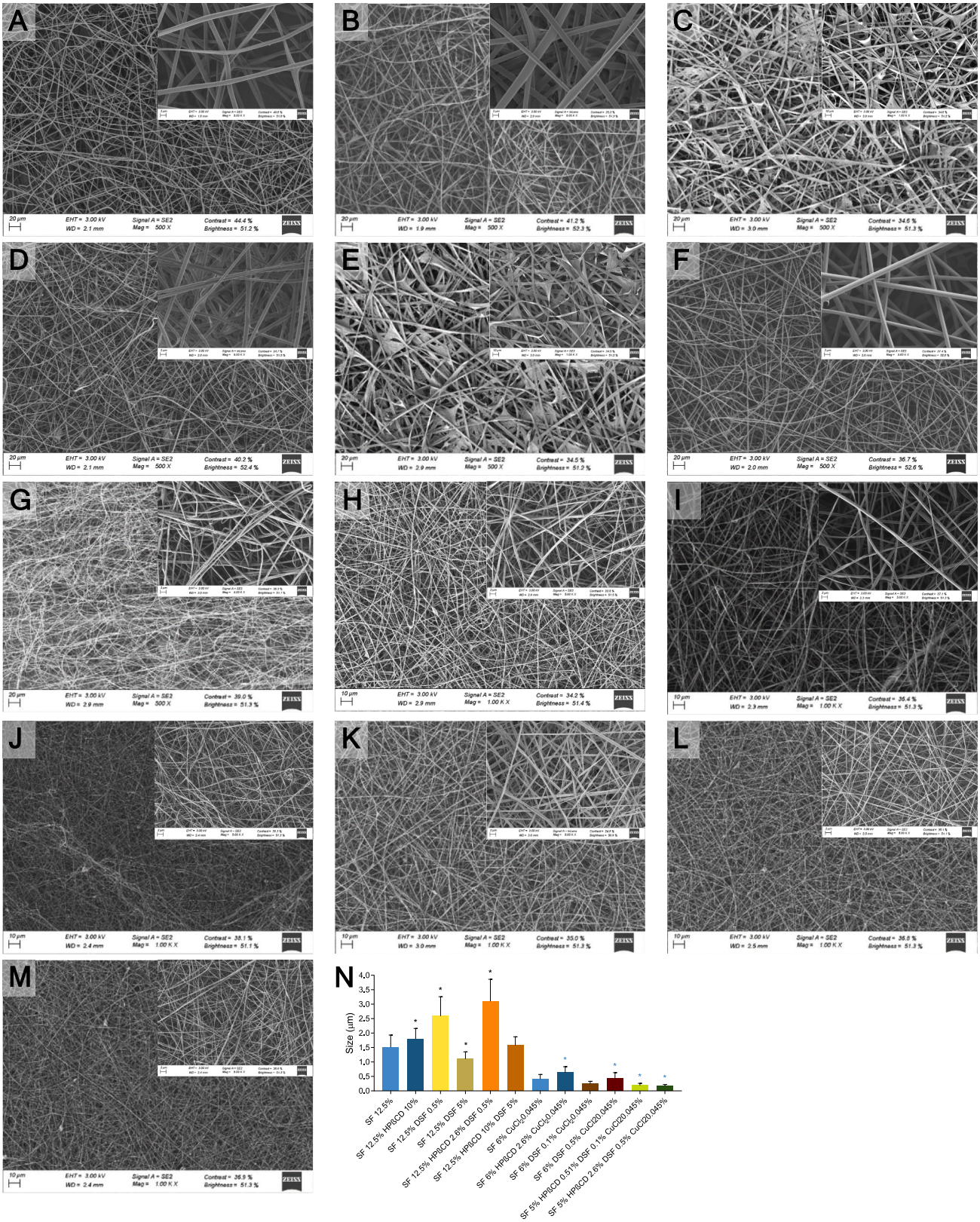

Fig. 1. SEM micrographs of fibers made from solutions in HFIP of (A) SF 12.5% (*w/v*); (B) SF 12.5% (*w/v*) HPβCD 10% (w/v); (C) SF 12.5% (w/v) DSF 0.5% (w/v); (D) SF 12.5% (w/v) DSF 5% (w/v); (E) SF 12.5% (w/v) HPβCD 2.6% (w/v) DSF 0.5% (w/v); (F) SF 12.5% (w/v) HPβCD 10% (*w/v*) DSF 5% (*w/v*); (G) SF 4% (w/v) $CuCl_2$ 0.45% (w/v); (H) SF 6% (*w/v*) $CuCl_2$ 0.045% (w/v); (I) SF 6% (w/v) HPβCD 2.6% (w/v) $CuCl_2$ 0.045% (w/v); (J) SF 6% (w/v) DSF 0.1% (w/v) $CuCl_2$ 0.045% (w/v); (K) SF 6% (w/v) DSF 0.5% (w/v) $CuCl_2$ 0.045% (w/v); (L) SF 5% (w/v) HPβCD 0.51% (w/v) DSF 0.1% (w/v) $CuCl_2$ 0.045% (w/v); and (M) SF 5% (w/v) HPβCD 2.6% (w/v) DSF 0.5% (w/v) $CuCl_2$ 0.045% (w/v); and (N) mean size and standard deviations (n = 200) of fibers diameters.

Table 2
Mechanical properties of SF fibers and $CuCl_2$ - SF fibers prepared with different contents in HPβCD, and DSF.

Fiber type	Young's modulus (MPa)	Tensile strength (MPa)	Elongation at break (%)
SF (12.5%)	7632	133.9	2.88
SF (12.5%) HPβCD (10%)	1079	26.20	1.55
SF (12.5%) DSF (0.5%)	2763	91.36	2.93
SF (12.5%) DSF (5%)	723	37.03	25.64
SF (12.5%) HPβCD (2.6%) DSF (0.5%)	301	18.72	6.53
SF (12.5%) HPβCD (10%) DSF (5%)	312	8.83	2.72
SF (6%) $CuCl_2$ (0.045%)	2807	101.14	5.87
SF (6%) HPβCD (2.6%) $CuCl_2$ (0.045%)	137	9.44	6.04
SF (6%) DSF (0.1%) $CuCl_2$ (0.045%)	3695	78.18	3.98
SF (6%) DSF (0.5%) $CuCl_2$ (0.045%)	83	25.66	9.91
SF (5%) HPβCD (0.51%) DSF (0.1%) $CuCl_2$ (0.045%)	4505	178.81	4.72
SF (5%) HPβCD (2.6%) DSF (0.5%) $CuCl_2$ (0.045%)	69	12.33	5.19

^{1} (C – O bending) and 1152 cm^{-1} (C – O bending/stretching) (assigned with numbers 1 and 2 in Fig. S7) were evident in all fibers containing HPβCD. The fibers that incorporated DSF showed a characteristic peak at 1496 cm^{-1}, assigned to C—H symmetrical deformation vibrations [22]. No other relevant bands were detected.

Surface polarity of the fibers was calculated from the measurements of contact angle of water, formamide and 1-bromonafthalene. Apolar, polar and hydrophobic components of the surface tension are summarized in **Table S2**. The two first components were evaluated using the Lifshitz-van de Waals component γ^{LW} and the Lewis acid-base component γ^{AB}. All fibers displayed a nonpolar component (γ^{LW}) close to 40 mJ/m^2 in good agreement with the fact of that the main structural component is a biopolymer [62]. The polar surface tension component (γ^{AB}) was calculated from the electron donor component (γ^-) and the electron acceptor component (γ^+) as reported previously [41]. The fibers with high contents in DSF showed high values of γ^+ due to the presence of electron-accepting ternary amide groups, whilst the fibers with high amounts of HPβCD displayed high values of γ^- owing to the presence of electron-donor OH groups.

SF fibers with or without $CuCl_2$ showed $\Delta G^{TOT} < 0$ mJ/m^2, indicating that the prepared fibers had a hydrophobic surface owing to hydrophobic character of SF β-sheet, and the addition of the Cu(II) did not change the surface polarity. Differently, $\Delta G^{TOT} > 0$ mJ/m^2 values were recorded for fibers incorporating HPβCD. Such an increase in hydrophilicity may promote cell migration while hindering bacterial adhesion [63]. Thereby, these hydrophilic electrospun mats could stimulate and promote tissue whilst avoiding nosocomial infections.

3.3. Disulfiram release profile

Release profiles of DSF from SF and SF-HPβCD fibers without $CuCl_2$ and with $CuCl_2$ are shown in Figs. 2 and 3, respectively. The tests were carried out in PBS of three different pH (7.4, 6.5, and 5.5) trying to mimic all the possible scenarios that the fibers could be exposed to, depending on the GB tumor resection location: "leading edge zone" that presents a normal pH 7.4, "cellular tumor zone" with a pH range values of 6.2 to 7, and "pseudo-palisading cell zone" of pH below 5.5 [64].

SF solely fibers showed slow release, with percentages of DSF released in the 1–5% range. The low amount of DSF released could be due to the fact that fibroin in beta conformation (verified in Section 3.2 FTIR) is hydrophobic and disulfiram is also a hydrophobic drug [25]. Changes in pH had minor impact on the amount of DSF released from SF solely fibers. A decrease in pH has been reported to trigger silk I to silk II transition [65], but this effect was not relevant in our case since the fibers were already prepared using silk II (beta-sheet, hydrophobic) conformation [66].

Differently, SF-HPβCD fibers presented a relevant burst release in all PBS media. The release started as soon as the fibers entered in contact with water, reaching 25–51% released in the first two hours, due to the solubilizing capability of HPβCD. The effect of the pH was again unnoticeable. These fibers suffered partial dissolution in PBS, being more evident for SF 12.5% HPβCD 10% DSF 5% than for SF 12.5% HPβCD 2.6% DSF 0.5% due to the highest content in HPβCD.

In the case of the fibers containing Cu(II), DSF chelation of Cu(II) can occur spontaneously in aqueous medium and is favored by a decrease in the pH, which facilitates the rupture of the S—S bond and the formation of diethyldithiocarbamate (DDC) [67]. The concentration of both the DSF released from the fibers and the $Cu(DDC)_2$ spontaneously formed during the release was monitored (Fig. 3). For all formulations, $Cu(DDC)_2$ was detected since the first time point. Cu(II)-containing fibers had nanometric size (<500 nm), with a large surface-area in contact with the release medium. It should be noted that all fibers were prepared using the same concentration of $CuCl_2$ 0.045% (*w/v*), but the final contents in Cu(II) of the solid mats were slightly different depending on the other components ratio (as indicated in Table 1**)** and ranged between 2.6 and 3.7 mg/g. Relevantly, the fibers combining Cu(II) with the lowest content in DSF (0.1% w/v) released the drug as a complex with Cu(II), namely as $Cu(DDC)_2$, which is the most active species against tumor cells and bacteria cells (Fig. 3A and C). These fibers were prepared with equimolar contents in Cu(II) and DSF, and the results confirmed the rapid decomposition of DSF in two molecules of DDC that chelate one Cu(II) ion, forming $Cu(DDC)_2$.

In the case of formulations prepared with 5 times more DSF (0.5% w/v), both DSF and $Cu(DDC)_2$ were detected in the medium (Fig. 3B and D). As observed for fibers without $CuCl_2$ (Fig. 2), incorporation of HPβCD significantly accelerated the release of intact DSF; the percentage released achieved 17% for SF 5% (*w/v*) HPβCD 2.6% (w/v) DSF 0.5% (w/v) $CuCl_2$ 0.045 (w/v) while it was approx. 5% released for SF 6% (w/v) DSF 0.5% (*w/v*) $CuCl_2$ 0.045 (*w/v*) fibers after 24 h in the medium.

Overall, a wide range of DSF/$Cu(DDC)_2$ amounts released were obtained in the first hours of the study, also showing the capability of the fibers to retain encapsulated DSF under the tested in vitro conditions. These mats displayed high stability and reproducibility since they released similar amounts of DSF and its chelate disregarding the changes in pH. Hence, these fibers may be potentially useful for supplying therapeutic amounts of DSF/$Cu(DDC)_2$ for GB treatment disregarding the state of this disease.

3.4. Hemolysis

A first screening of biocompatibility was carried out testing the compatibility with human blood (**Fig. S8**). The fibers did not cause hemolysis. Even the SF 12.5% (w/v) HPβCD 10% (w/v) DSF 5% (w/v) fibers that released the highest concentrations of disulfiram had values well below the 5% hemolysis, set as the safe threshold.

3.5. Antimicrobial activity

The antimicrobial activity of the fibers was tested against *S. aureus* and *P. aeruginosa* (Fig. 4). SF 12.5% (w/v) HPβCD 10% (w/v) DSF 5% (w/v) fibers displayed the most intense antimicrobial activity against *S. aureus* reaching a reduction of up to 4.84 Log_{10} (CFU/mL), which can be clearly attributed to the role of HPβCD as solubilizing agent and promoter of DSF release. SF 12.5% (*w/v*) DSF 5% (w/v) fibers (without HPβCD) showed a slight antimicrobial effect with a reduction of only

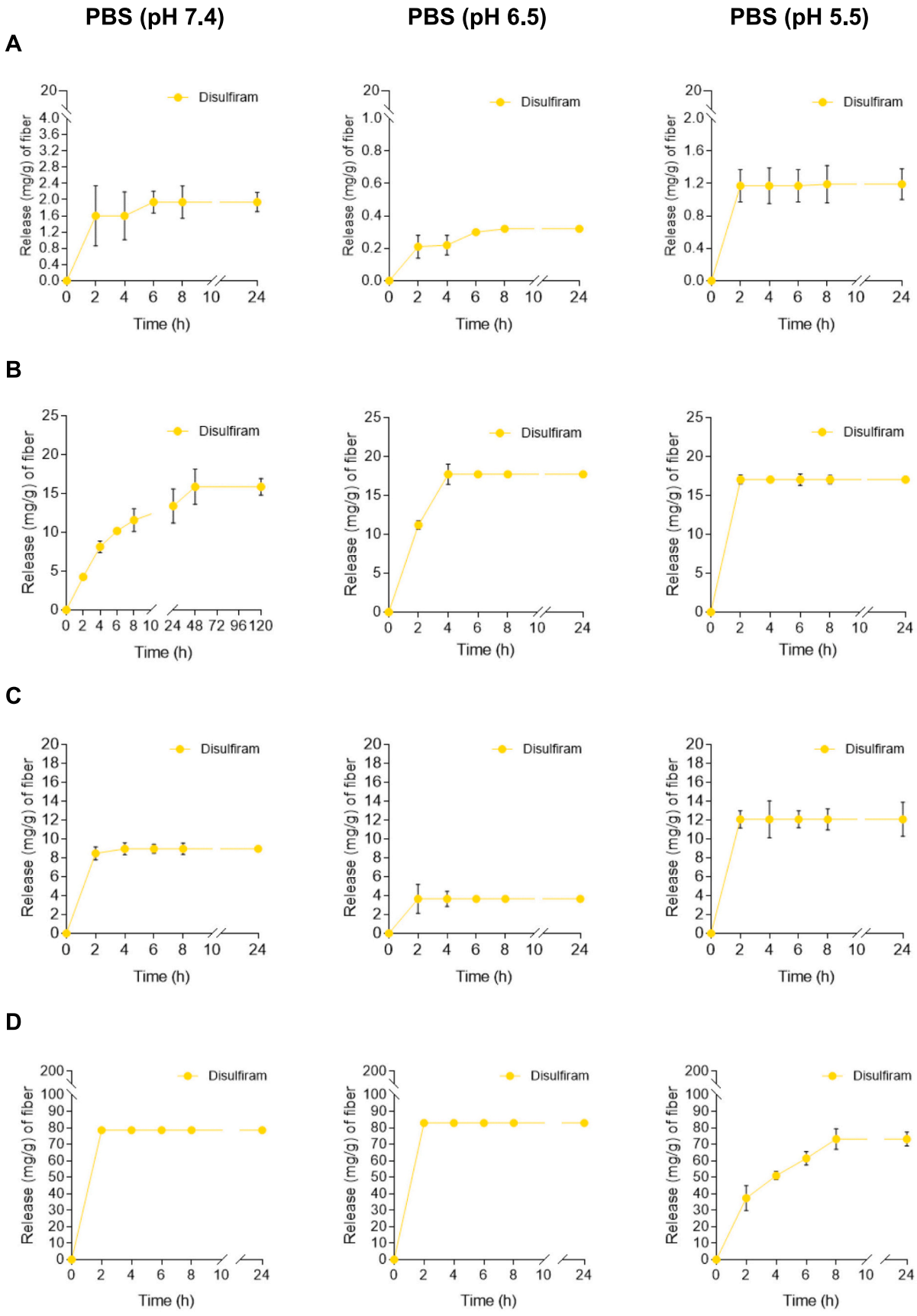

Fig. 2. Release profile of disulfiram from silk fibroin fibers prepared with and without HPβCD in PBS at different pHs under 100 rpm and at 37 °C. **(A)** SF 12.5% (*w/v*) DSF 0.5% (w/v), (**B**) SF 12.5% (*w/v*) DSF 5% (*w/v*), (**C**) SF 12.5% (*w/v*) HPβCD 2.6% (w/v) DSF 0.5% (w/v), and (**D**) SF 12.5% (w/v) HPBCD 10% (w/v) DSF 5% (*w/v*).

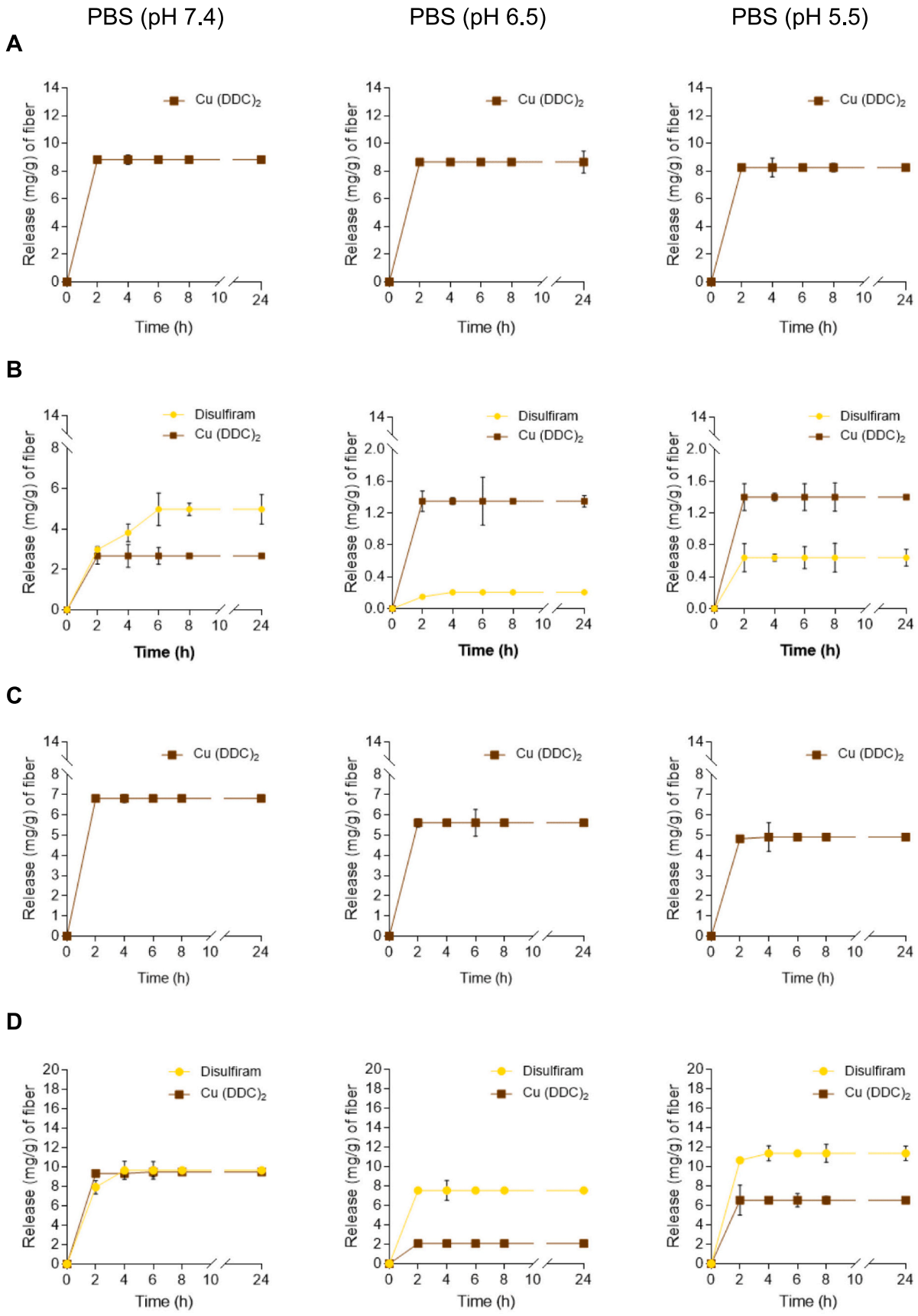

Fig. 3. Release profile of disulfiram and its chelate from silk fibroin fibers loaded with different concentrations of HPβCD, disulfiram and $CuCl_2$ (**A**) SF 6% (*w/v*) DSF 0.1% (w/v) $CuCl_2$ 0.045% (*w/v*), (**B**) SF 6% (*w/v*) DSF 0.5% (w/v) $CuCl_2$ 0.045% (w/v), (**C**) SF 5% (w/v) HPβCD 0.51% (w/v) DSF 0.1% (w/v) $CuCl_2$ 0.045% (w/v), and (**D**) SF 5% (w/v) HPBCD 2.6% (w/v) DSF 0.5% (w/v) $CuCl_2$ 0.045% (w/v) in PBS at different pHs under 100 rpm and at 37 °C.

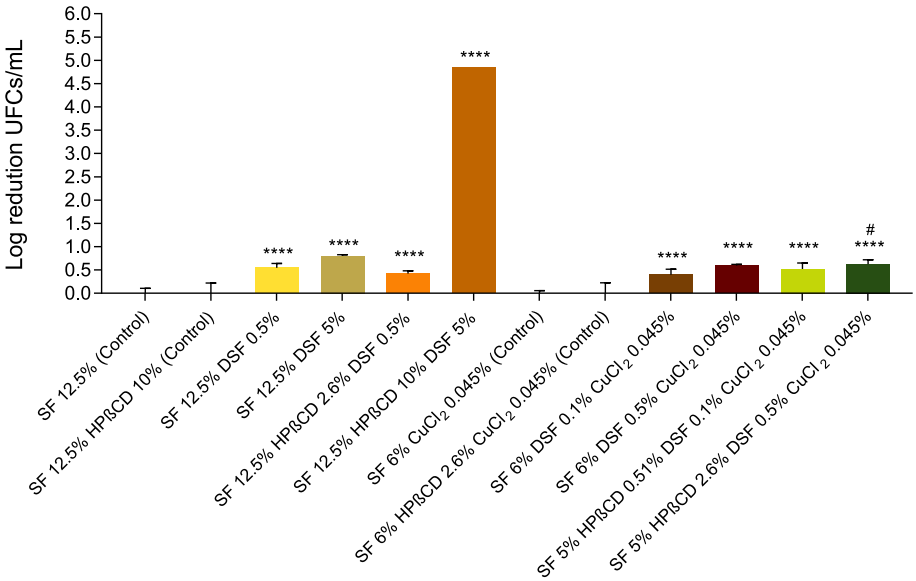

Fig. 4. Antimicrobial activity of SF fibers prepared with different concentrations of HPβCD, disulfiram, and $CuCl_2$ against *S. aureus*, in terms of reduction of culturable cells (log (CFU/mL) reduction) after 24 h of incubation at 37 °C under gentle agitation. Mean ± standard deviation, $n = 4$. Asterisk (*) was used to compare the antimicrobial activity of the fibers against the SF 12.5% (control fiber) and the number sign (#) was used to compare the antimicrobial activity of SF fibers without copper and with copper loaded with same content in DSF and HPβCD. * $p < 0.05$, ** $p < 0.005$, *** $p < 0.001$ and **** $p < 0.0001$.

0.80 Log_{10} (CFU/mL).

Interestingly, the fibers loaded with DSF 0.5% (*w/v*) displayed a similar antimicrobial activity if compared with SF 12.5% (w/v) DSF 5% (w/v) fibers (no statistically significant differences). The presence of $CuCl_2$ slightly increased the antimicrobial activity: SF 6% (w/v) DSF 0.5% (w/v) $CuCl_2$ 0.045% (w/v) caused a reduction of 0.59 Log_{10} (CFU/mL) and SF 5% (w/v) HPβCD 2.6% (w/v) DSF 0.5% (w/v) $CuCl_2$ 0.045% (w/v) caused a reduction of 0.62 Log_{10} (CFU/mL).

SF fibers loaded with lower amounts of DSF (0.1% w/v) did not show activity against *S. aureus* (< 0.5 log microbial growth reduction): SF 6% (w/v) DSF 0.1% (w/v) $CuCl_2$ 0.045% (w/v) with 0.39 Log_{10} (CFU/mL), whilst SF 5% (w/v) HPβCD 0.51% (w/v) DSF 0.1% (w/v) $CuCl_2$ 0.045% (w/v) had 0.52 Log_{10} (CFU/mL). Clearly both HPβCD (promoting DSF release) and Cu(II) (forming a chelate with DSF) enhanced the activity of the fibers against *S. aureus* [22,68].

In the case of *P. aeruginosa,* SF 12.5% (*w/v*) HPβCD 10% (w/v) DSF 5% (w/v) fibers were again the most active ones, reaching a reduction of up to 5.96 Log_{10} (CFU/mL), compared to SF 12.5% (w/v) DSF 5% (w/v), which were still active and ranked the second ones, but caused a reduction of 0.75 Log_{10} (CFU/mL) (Fig. 5). The other fibers did not cause antimicrobial effects, except for SF 5% (w/v) HPβCD 2.6% (w/v) DSF 0.5% (w/v) $CuCl_2$ 0.045% (w/v) with 0.47 Log_{10} (CFU/mL). This last fiber showed the best antimicrobial activity of Cu(II)-containing fibers, displaying statistical differences ($^{\#}p < 0.05$) with similar fibers prepared in the absence of $CuCl_2$.

Results obtained in the antimicrobial tests agreed with the release

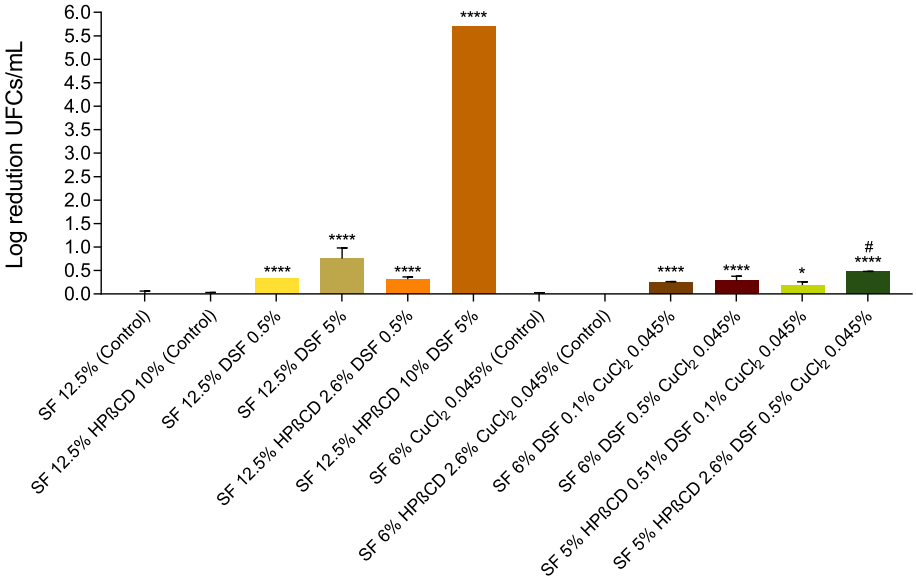

Fig. 5. Antimicrobial activity of SF fibers prepared with different concentrations of HPβCD, disulfiram, and $CuCl_2$ against *P. aeruginosa*, in terms of reduction of culturable cells (log (CFU/mL) reduction) after 24 h of incubation at 37 °C under gentle agitation. Mean ± standard deviation, n = 4. Asterisk (*) was used to compare the antimicrobial activity of the fibers against the SF 12.5% (control fiber) and number sign (#) was used to compare the antimicrobial activity of SF fibers without copper and with copper loaded with same content in DSF and HPβCD. * $p < 0.05$, ** $p < 0.005$, *** $p < 0.001$ and **** $p < 0.0001$.

tests since the best results were found for SF 12.5% (w/v) HPβCD 10% (w/v) DSF 5% (w/v) that released the highest amounts of disulfiram. Overall, DSF was revealed as a potential drug in infections or as a prophylactic agent with good antimicrobial properties.

3.6. Anticancer activity on glioblastoma cells

As a first step, the effect of DSF on survival of glioblastoma cells was evaluated through a dose-response study on different murine and human glioblastoma cell lines (Fig. 6). The antitumoral activity of DSF in the presence of 1 μM of copper in the medium strongly reduced the viability (resazurine assay) of glioblastoma cell lines at 24 and 48-h treatment (Fig. 6A). The concentration needed to inhibit 50% of cell viability (IC_{50}) for GL261 was 0.12 μM after 24 and 48 h of treatment, meanwhile for the human glioblastoma cell lines (U-87MG and U-251MG) IC_{50} was 0.20 μM and 0.30 μM at 24 h and decreased to 0.12 μM and 0.15 μM at 48 h respectively.

Alongside these findings, the antiproliferative potential of DSF

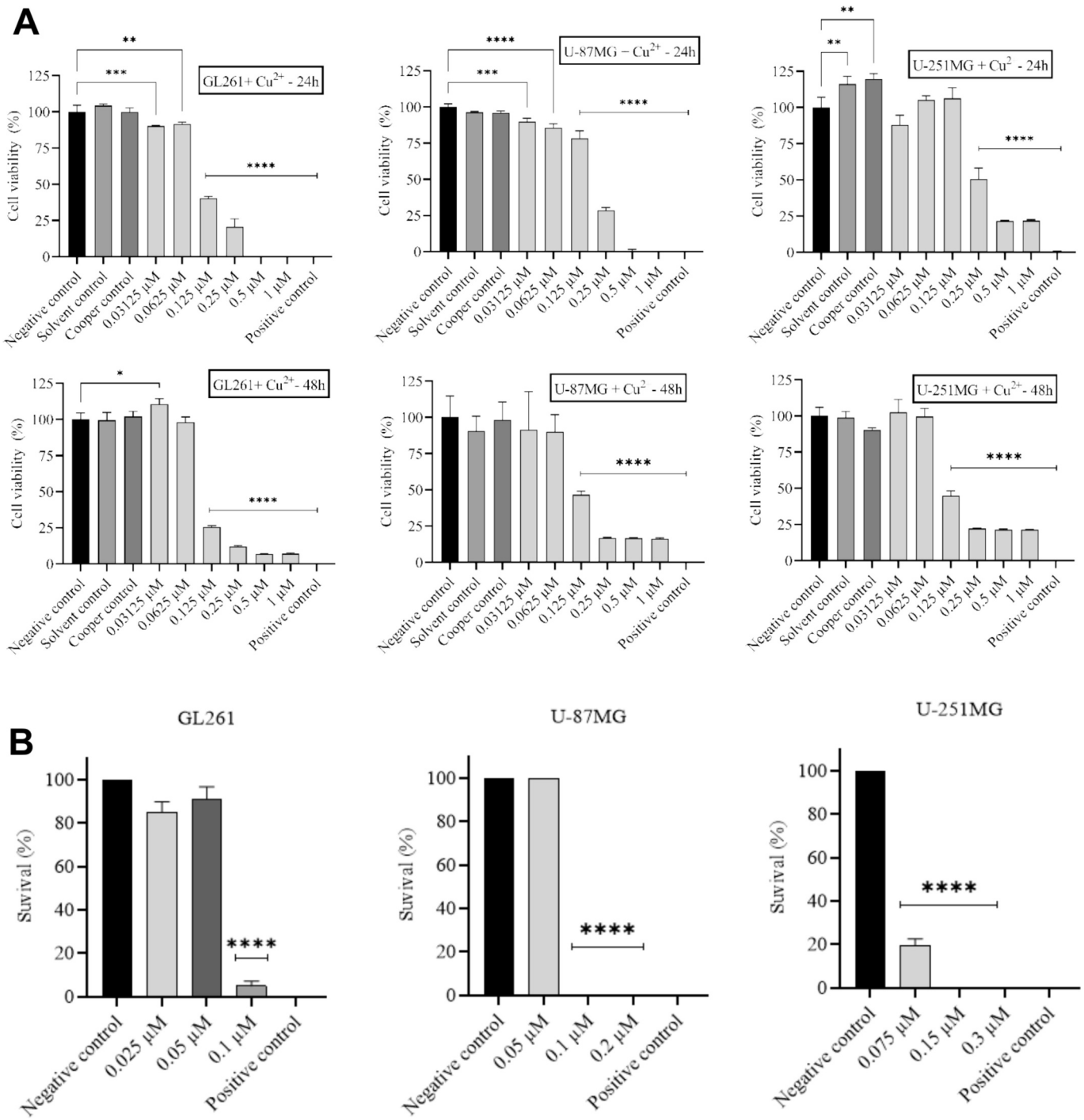

Fig. 6. Effect of disulfiram combined with cooper as an anticancer agent on glioblastoma cells. **(A)** Percentage of cell viability after exposition to different dose of disulfiram (0.03–1 μM) with 1 μM cooper in the medium, on GL261 (murine glioblastoma cell line), U-87MG and U-251MG (human glioblastoma cell line) after 24 or 48-h of treatment. **(B)** Percentage of colonies survival after 24 h of treatment of disulfiram (concentrations based on IC_{50}) in combination with 1 μM of copper, on GL261, U-87MG and U-251MG. Mean ± standard deviation, triplicate * $p < 0.05$, ** $p < 0.005$, *** $p < 0.001$ and **** $p < 0.0001$.

combined with copper was measured by studying the capacity of glioblastoma cells to form cell clones after treatment (done only after two hours of recovery after seeding of the cells) by using the Giemsa stain technique [58]. As evidenced on Fig. 6B, this capacity was strongly decreased at concentrations greater than IC_{50} for GL261 cells, while it was completely abolished in the human glioblastoma cell lines (U-87MG and U-251MG) at 0.10 μM and 0.15 μM, respectively. These results suggest a global effect of DSF beyond a particular subtype of cells within these heterogeneous cell lines. Results obtained were consistent with previous reports on the cytotoxic effect of DSF on glioblastoma cell lines U-87MG, U-251MG, and U-373MG [69], which evidenced that non-toxic copper is necessary to obtain this cytotoxic effect on cancer cells. In fact, DSF forms a complex with Cu(II) ions that inhibits the proteasome activity and NF- κB signaling, which causes the death of cancer cells [11,70,71]. These results show a potential use of DSF alone or in combination with other therapeutics for the development of a new therapy.

To gain further insight into the potential toxic effect of DSF beyond the anticancer properties in the central nervous system, and for future preclinical investigations, studies were also conducted on murine cells of the CNS that divide slowly in neutral conditions, astrocytes (to compare with GL261). As shown in Fig. 7A, the treatment had no effect on this type of cell. Differently, on murine fibroblast (NIH-3T3 cell line) (Fig. 7A), which were still in cell cycle phase, DSF showed cytotoxic effects. This reveals a potential toxicity of DSF with copper on dividing cells. Regarding these results, potential toxic effects of the systemic administration of a high dose of DSF in the alcoholism treatment can be predicted. In our case, the locoregional and controlled administration of the treatment directly in the brain is an undeniable advantage.

To investigate more thoroughly potential synergies between the conventional treatment of glioblastoma which include beam radiation and the use of DSF, a study of association of treatment with a 16GY dose of radiation was conducted. Relevantly, DSF preserved its activity during irradiation, with a potentiation of the effects at 0.06 μM on GL261, while maintaining his harmlessness on astrocytes on which beam radiations had no effects (Fig. 7B). There is a slight toxicity of irradiation on murine fibroblasts (NIH-3T3) but no synergic effect with DSF on this cell line (Fig. 7B). These results demonstrate that for a development of a combined therapeutic strategy (DSF + radiotherapy), it is possible to optimize the intensity and frequency of irradiation to have the best effect of the combination (synergy and lack of toxicity).

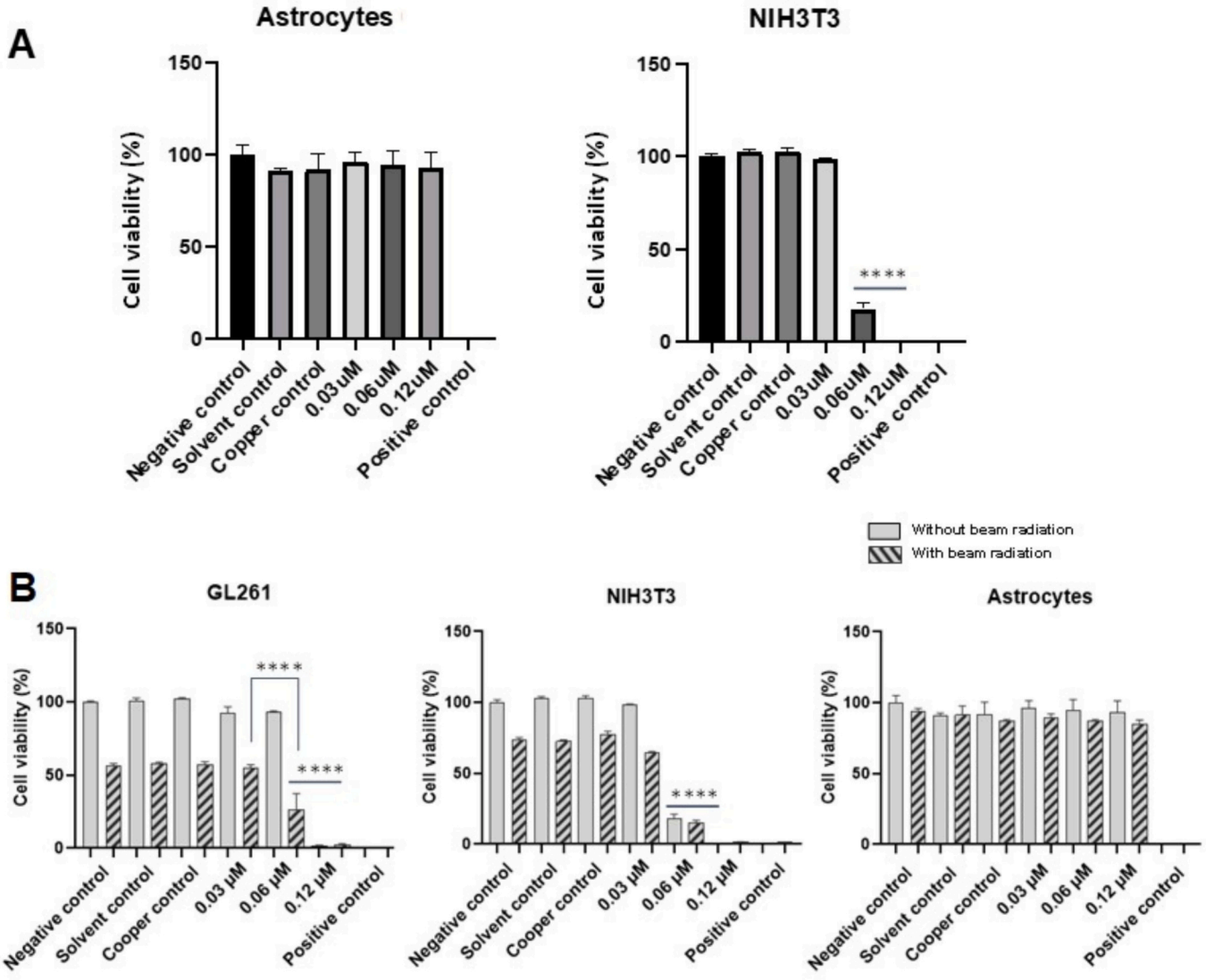

Fig. 7. Disulfiram toxicity on cycling cells (NIH-3T3), central nervous system non cycling cells (astrocytes) and combination of treatment with beam radiation. **(A)** Percentage of cell viability after exposition to different dose of disulfiram (0.03–0.12 μM) with 1 μM cooper in the medium, on NIH-3T3 and mouse primary astrocytes after 24 h of treatment. **(B)** Percentage of cell viability after exposition to disulfiram (0.03–0.12 μM) with cooper in combination with irradiation (16GY) on GL261, NIH-3T3 and mouse primary astrocytes. Mean ± standard deviation, triplicate * $p < 0.05$, ** $p < 0.005$, *** $p < 0.001$ and **** $p < 0.0001$.

Considering all these results, the possibility of administrating in safe and controlled manner DSF in the CNS was then investigated using the developed SF fibers (Fig. 8).

SF solely fibers (12.5%) did not cause any effect on cells. When DSF at 5% was added to the SF fibers, there was also a lack of effect on GL261 cells, which could be explained by the small amount of DSF released after 24 h of treatment (as recorded in the release tests, Fig. 2**)**. Lowering DSF proportion in the fiber remarkably promoted the cytotoxic effect, either in the absence or in the presence of HPβCD (Fig. 8), as the fibers were more hydrophilic, and the release was facilitated. DSF is highly hydrophobic and an increase in DSF dose makes the system less prone to release the drug. In the absence of DSF, the presence of $CuCl_2$ in the fibers did not trigger any cytotoxic effect on cancer cells. Differently, SF fibers prepared combining DSF, Cu(II) and HPβCD showed a strong antitumoral effect, with almost 100% of cell death after 24 h of treatment.

Thus, SF 5% (*w/v*) HPßCD 2.6% (w/v) DSF 0.5% (w/v) $CuCl_2$ 0.045% (w/v) and SF 5% (w/v) HPβCD 0.51% (w/v) DSF 0.1% (w/v) and $CuCl_2$ 0.045% (w/v) fibers seems to be the best option to have a complete cytotoxic effect on glioblastoma cells.

3.7. In vivo medium-term biocompatibility of SF-fibers: Locoregional histological analysis

A thorough in vivo anatomocytopathological study was conducted on naïve rats to investigate the locoregional cellular responses following the implantation of SF-fibers in healthy brain parenchyma. Two types of fibers, namely SF 12.5% (w/v) HPβCD 2.6% (w/v) DSF 0.5% (w/v) and SF 5% (w/v) HPβCD 2.6% (w/v) DSF 0.5% (w/v) $CuCl_2$ 0.045% (w/v), were directly implanted into a resection cavity in the cortex. The latter fibers were chosen considering together the antimicrobial and the antitumoral activities, while the former ones without Cu(II) were chosen as a reference to detect potential toxicity problems ascribed to the metal ions and the formation of the $Cu(DCC)_2$ chelate. Both types of fibers were verified to significantly reduce the proteasome activity in glioblastoma cells (**Fig. S9**) and thus may act as proteasome inhibitors able to alter the cell cycle and cause apoptosis of GB cells [14]. The surgery mimicked GB resection and implantation of a device that, if most tumor was removed, would be in contact with the healthy brain [32].

One week after the implantation, brains were collected and stained with HE to investigate cellular and tissular responses that can occur following SF-fiber implantation in the cortex in comparison to the cavity control situation. As described in many brain surgical procedures, the results presented in Fig. 9A and B indicated a mild but well identified inflammatory response in the control group. It was characterized by the presence of chronic inflammatory cells that include macrophages, lymphocytes and the occurrence of neoangiogenesis supporting tissue healing. Interestingly, no differences in terms of tissue response to surgery were noticed while comparing SF-fibers containing disulfiram at 0.5% and HPβCD to the cavity control. The recruitment of inflammatory cells was very similar with mild colonization of the tissue and no apparent signs of toxicity (Fig. 9B). In contrast, when using fibers containing disulfiram with HPβCD and $CuCl_2$, a higher global response was observed with more macrophages, lymphocytes recruited in several animal while being less homogeneous as in the other animal groups. Among the five rats included in this group, two exhibited an enhanced response, with a spread of inflammation and a notable presence of apoptotic bodies (Fig. 9B). All other tested parameters remained the same as for the control cavity (Fig. 9A).

This study on implantability and behavior of the brain parenchyma with respect to implanted SF-fibers does not prejudge the best possible candidate in terms of effectiveness but reflects a possible better acceptance of SF-fibers without Cu(II). It should also be noted that the very nature of fibers containing Cu(II) makes them mechanically more complex to handle.

3.8. In vivo evaluation of the effect of DSF fibers on residual GB cells growth

As a final step, a prospective, exploratory study was carried out to investigate the impact of DSF fibers in the brain of tumor-bearing animals to generate new hypotheses for potential clinical applications. Due

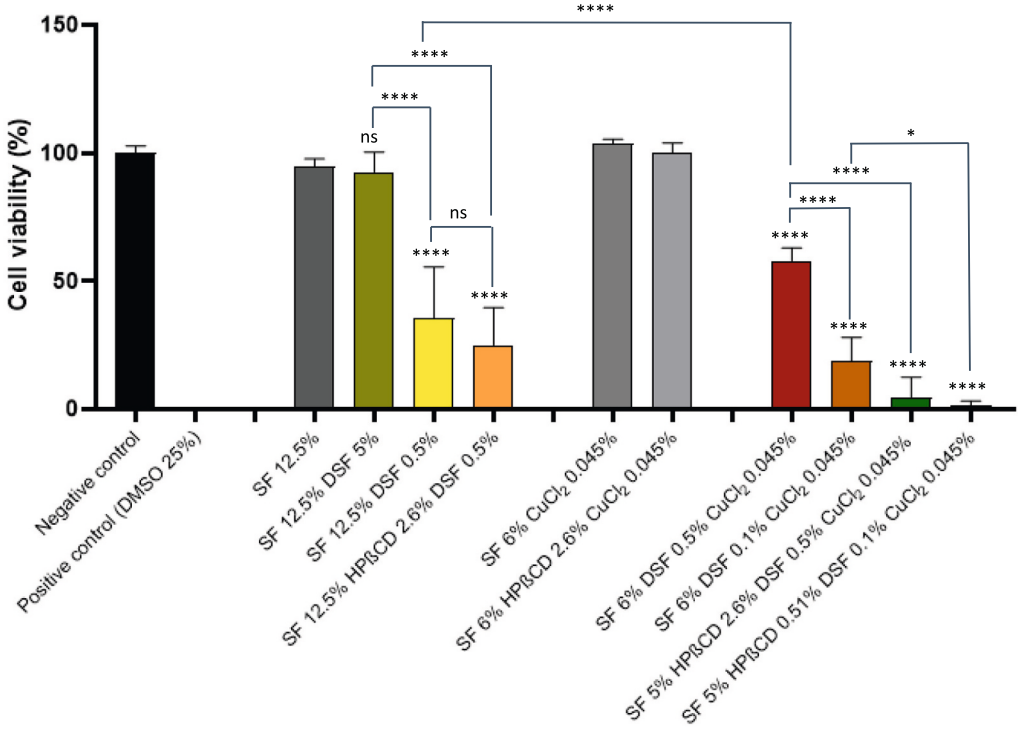

Fig. 8. Effect on cell viability of SF fibers prepared with different concentrations of HPβCD, disulfiram, and $CuCl_2$ after 24 h of treatment on GL261. Mean ± standard deviation, $n = 3$ * $p < 0.05$, ** $p < 0.005$, *** $p < 0.001$ and **** $p < 0.0001$.

A

Cavity control n=5	SF 12.5% HPβCD 2.6% DSF 0.5% n=4	SF 5% HPβCD 2.6% DSF 0.5% $CuCl_2$ 0.045% n=5	[- -/+ + ++ +++]
- - - - -	- - - -	- - - - -	Multinucleated Giant cells
-/+ + - - -	- -/+ + -	- - + -/+ ++	Acute inflammatory cells (PMN cells)
- - - - -	- - - -	- - - - ++	Cellular debris and apoptotic bodies
+ ++ ++ ++ ++	++ ++ ++ +	++ + +++ ++ +++	Chronic inflammatory cells
+ ++ + ++ +	+ + + +	++ + +++ ++ +	Neoangiogenesis
- - - - -	- - - -	- - - - -	Haemorrhage
- -/+ - - -	- - - -/+	+ - -/+ + -/+	Hemosiderin
- - - - -	-/+ - - -	-/+ - - - -	Mineralization

B

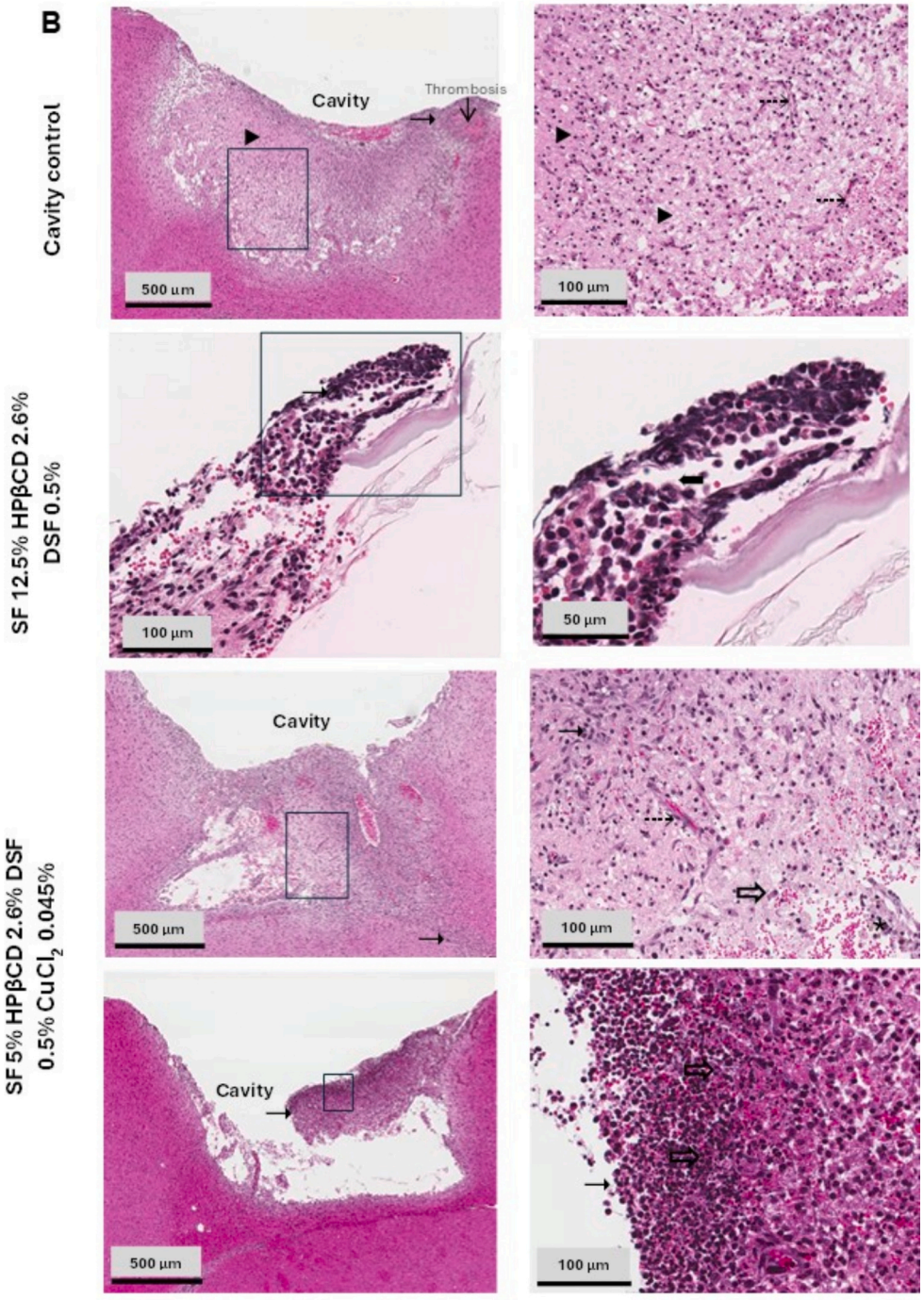

(caption on next page)

Fig. 9. In vivo assessment of the impact of disulfiram fibers implantation in rat's brains. **(A)** Characterization of the in vivo cellular response to implanted fibers in the rat brain cortex. Scores are as follows: (−) = nil, (−/+) = rare, (+) = mild, (++) = moderate, and (+++) = marked. **(B)** Histological (H&E) staining (nuclei: blue/purple; cytoplasm: pink) images revealed the inflammatory response across the different study conditions one-week post-surgery. Symbols are as follows: Lymphocytes (→), Macrophages (▶), PMN cells (➡), neoangiogenesis (⇢), Hemosiderin (*), Apoptotic bodies (⇨). Interrupted-line bordered images are magnifications of the smaller squares indicated in their respective left images. (For interpretation of the references to colour in this figure legend, the reader is referred to the web version of this article.)

to the study's exploratory nature, it was challenging to predict outcomes or determine the optimal clinical use, whether during tumor resection or for recurrence treatment. Given that carmustine is not routinely used, and limitations exist with current treatments like the Stupp protocol and temozolomide resistance, we did not combine DSF fibers with radiotherapy, carmustine or temozolomide. Instead, we focused on DSF monotherapy, adhering to the 3Rs principles for animal research.

To evaluate the specific effects of DSF fibers on tumor development from residual glioblastoma cells present within resection cavity margins, a brain resection cavity model with a pericavitary cell implantation was developed [32]. The MRI analyses revealed that the various treatments had no notable effects on tumor development from the cavity margins (Fig. 10). The animals were euthanized at day 20 and the tumor volumes were calculated. It should be noted, however, that two out of four animals treated with DSF + Cu^{2+} fibers (SF 5% HPβCD 2.6% DSF 0.5% $CuCl_2$ 0.045%) presented increased tumor volumes. This last result suggests that for subsequent efficacy analyses on larger cohorts in association with radiotherapy or combined chemotherapy, copper should probably not be added to the DSF fibers, contrary to what may have been useful in vitro. It should be noted that cancer cells already exhibit higher levels of intracellular Cu (2–3-fold) compared with healthy cells [13]. Also, the neurotoxicity of higher copper concentrations has been documented [72] while the effects of co-treatment in association with different strategies (addition, chelation) have given multiple and/or contradictory results [73,74].

Finally, hematoxylin-eosin histological analysis on brain section at day 20 (not shown) revealed that all tumors, regardless of the condition, were well-defined, densely cellular, and slightly fasciculated. They consisted of medium-sized cells, with a few giant cells sometimes exhibiting multiple nuclei, as well as minimal necrotic foci and numerous mitoses. Some acidophilic necrotic foci were also observed. Exceptionally, leptomeningeal invasion was noted in one control animal, and ventricular dissemination spaces were observed in one case among the animals treated with DSF + Cu^{2+} fibers. Therefore, no significant difference was observed in tissue characteristics after treatment, regardless of the condition, within this small sample. These results taken as a whole demonstrate both the feasibility of such an application of DSF fibers and the interest of being able to evaluate them in different therapeutic contexts notably in combination with radiation treatments (including external beam but also flash or vectorized alpha and beta radiotherapy) to treat residual disease within the cavity margins with the aim of limiting or preventing recurrences. Mechanisms involving ROS production and the impact of DSF on the protasome in this context would also be of interest.

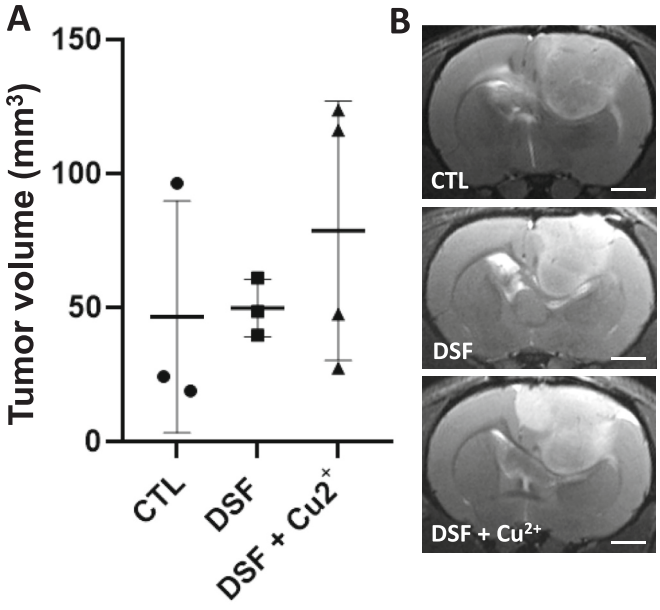

Fig. 10. In vivo evaluation of the effect of DSF fibers on residual GB cells growth. (A) Graph representing tumor volumes calculated from MRI images on animals subjected to pericavitary cell implantation models including the control cavity (CTL), the cavity implanted with DSF fibers (SF 12.5% HPβCD 2.6% DSF 0.5%) and the cavity implanted with DSF + Cu^{2+} fibers (SF 5% HPβCD 2.6% DSF 0.5% $CuCl_2$ 0.045%). (B) MRI images (coronal sections) on representative animals. Bars = 2 mm.

4. Conclusions

Electrospun fibers prepared using freeze-dried SF as main component revealed to be highly versatile to encapsulate considerable amounts of DSF and HPβCD. Incorporating small proportions of Cu(II) in the fibers allowed reducing the dose of DSF. However, the production of electrospun fibers of SF with Cu(II) was quite challenging due to the lack of solubility of the inorganic salt in HFIP and the strong interaction between both components, which caused the precipitation of SF. This problem was overcome tuning SF and Cu(II) concentration and using DMF as cosolvent and resulted in the obtaining of nanometric fibers of adequate mechanical properties.

Both HPβCD and $CuCl_2$ were shown to play very relevant roles in the control of DSF release and the in-situ formation of the DSF-copper chelate, which ultimately determined the performance of the fibers as antimicrobial and antitumor implantable devices. Relevantly, the release rate of DSF and in situ formation of $Cu(DDC)_2$ were not altered by pH changes in the range typical of healthy and tumoral brain tissues. The fibers allowed obtaining a good synchronization of the supply of the two therapeutic agents together from the same formulation, overcoming the need of administering DSF and Cu(II) in separate. The increased potency of DSF at lower concentrations when combined with SF fibers prepared with HPβCD and copper is particularly noteworthy. These findings suggest that DSF delivery and bioavailability can be significantly optimized through these combinations, which may also allow for more precise dosing. The interaction with copper, given DSF known role in copper chelation and the generation of reactive oxygen species, might also provide a mechanistic explanation for this enhanced activity. As a limitation of the developed formulations, it should be mentioned that SF 5% HPβCD 2.6% DSF 0.5% $CuCl_2$ 0.045% fibers are weaker than the others, which makes their handling more difficult. On the other hand, they are the ones that best imitate the biological softness of the brain. Thus, the balance in mechanical properties requires further studies.

Of outmost importance from a regulatory perspective, the fibers were blood-compatible and did not trigger any toxic effect when loaded with DSF or $CuCl_2$ in separate. Moreover, selectivity against tumor cells compared to normal astrocytes is particularly relevant. This specificity is significant in the context of brain cancer treatment, where preserving healthy tissue is paramount. The observed toxicity on fibroblasts, in contrast, suggests that DSF may have a broader range of cellular targets, linked to differential metabolic pathways or variations in copper

metabolism between cell types. Exploring this mechanism further could provide valuable insights. Additionally, the fibers are biodegradable and when its therapeutic purpose is complete (i.e., the release of DSF), all components could be reused by a variety of cells; for example, SF amino acids could be utilized for myriads of process (e.g. energy obtention), HPβCD can capture toxic substances forming inclusion complexes to be cleared from the body, and Cu(II) could be stored by astrocytes and reused to maintain a correct homeostasis or participate in neuronal synapses.

The small prospective study assessing the feasibility of GB treatment indicates that DSF-loaded electrospun fibers alone may be insufficient, suggesting the need for combination with existing therapies. The study also revealed potential in vivo disadvantages of copper addition while confirming the system's safety and localized antitumor effects, which warrant further investigation.

Funding

The work was supported by MCIN [PID 2020-113881RB-I00/AEI/10.13039/501100011033], Spain, FEDER, Xunta de Galicia [ED431C 2024/09], the Institut National de la Santé et de la Recherche Médicale (INSERM), the University of Angers and by the French National Agency for Research (ANR) under the frame of EuroNanoMed III (project GLIOSILK) [ANR-19-ENM3-0003-01] (to EG and CAL), and the "France 2030 Investment Plan" Labex Iron [ANR-11-LABX-18- 01] (to EG, funding of MD). It was additionally related to: the "Région Pays-de-la-Loire" under the frame of the Target'In project (to EG); the "Ligue Nationale contre le Cancer" and the "Comité Départemental de Maine-et-Loire de la Ligue contre le Cancer" (CD49) under the frame of the FusTarG project (to EG) and the "Tumour targeting, imaging and radiotherapies network" of the "Cancéropôle Grand-Ouest" (France).

CRediT authorship contribution statement

Iago Gonzalez-Prada: Writing – review & editing, Writing – original draft, Visualization, Validation, Software, Methodology, Investigation, Formal analysis, Data curation, Conceptualization. **Arthur Barcelos Ribeiro:** Writing – review & editing, Visualization, Methodology, Investigation, Formal analysis. **Marine Dion:** Writing – review & editing, Visualization, Validation, Software, Methodology, Investigation, Formal analysis, Data curation, Conceptualization. **Beatriz Magariños:** Writing – review & editing, Supervision, Methodology, Investigation, Formal analysis, Conceptualization. **Clémentine Lapoujade:** Writing – review & editing, Validation, Methodology, Investigation, Formal analysis. **Audrey Rousseau:** Writing – review & editing, Visualization, Resources, Methodology, Investigation, Formal analysis, Conceptualization. **Angel Concheiro:** Writing – review & editing, Writing – original draft, Supervision, Resources, Project administration, Investigation, Funding acquisition, Conceptualization. **Emmanuel Garcion:** Writing – review & editing, Writing – original draft, Supervision, Resources, Project administration, Investigation, Funding acquisition, Formal analysis, Data curation, Conceptualization. **Carmen Alvarez-Lorenzo:** Writing – review & editing, Writing – original draft, Validation, Supervision, Resources, Project administration, Investigation, Funding acquisition, Formal analysis, Conceptualization.

Declaration of competing interest

The authors declare that they have no known competing financial interests or personal relationships that could have appeared to influence the work reported in this paper.

Appendix A. Supplementary data

Supplementary data to this article can be found online at https://doi.org/10.1016/j.jconrel.2025.113615.

Data availability

Data will be made available on request.

References

[1] D.N. Louis, A. Perry, P. Wesseling, D.J. Brat, I.A. Cree, D. Figarella-Branger, C. Hawkins, H.K. Ng, S.M. Pfister, G. Reifenberger, R. Soffietti, A. von Deimling, D. W. Ellison, The 2021 WHO classification of tumors of the central nervous system: a summary, Neuro-Oncology 23 (8) (2021) 1231–1251, https://doi.org/10.1093/neuonc/noab106.

[2] T.S. van Solinge, L. Nieland, E.A. Chiocca, et al., Advances in local therapy for glioblastoma — taking the fight to the tumour, Nat. Rev. Neurol. 18 (2022) 221–236, https://doi.org/10.1038/s41582-022-00621-0.

[3] M. Weller, W. Wick, K. Aldape, M. Brada, M. Berger, S.M. Pfister, R. Nishikawa, M. Rosenthal, P.Y. Wen, R. Stupp, G. Reifenberger, Glioma, Nat. Rev. Dis. Primers 1 (2015) 15017, https://doi.org/10.1038/nrdp.2015.17.

[4] F. Ragucci, F. Sireci, F. Cavallieri, J. Rossi, G. Biagini, G. Tosi, C. Lucchi, R. Molina-Pena, N.H. Ferreira, M. Zarur, A. Ferreiros, W. Bourgeois, F. Berger, M. Abal, A. Rousseau, F. Boury, Insights into healthcare professionals' perceptions and attitudes toward Nanotechnological device application : what is the current situation in glioblastoma research ? Biomedicines 11 (2023) 1854, https://doi.org/10.3390/biomedicines11071854.

[5] C.Y. Foo, N. Munir, A. Kumaria, Q. Akhtar, C.J. Bullock, A. Narayanan, R.Z. Fu, Medical device advances in the treatment of glioblastoma, Cancers 14 (2022) 5341, https://doi.org/10.3390/cancers14215341.

[6] T. Iqbal, P. Rewatkar, A. Ahmed-Cox, I. Saeed, F.M. Mansfeld, R. Kulshreshtha, T. Kumeria, D.S. Ziegler, M. Kavallaris, R. Mazzieri, A. Popat, Frontiers in the treatment of glioblastoma: past, present and emerging, Adv. Drug Deliv. Rev. 171 (2021) 108–138, https://doi.org/10.1016/j.addr.2021.01.012.

[7] S. Pushpakom, F. Iorio, P.A. Eyers, K.J. Escott, S. Hopper, A. Wells, A. Doig, T. Guilliams, J. Latimer, C. McNamee, A. Norris, P. Sanseau, D. Cavalla, M. Pirmohamed, Drug repurposing: progress, challenges and recommendations, Nat. Rev. Drug Discov. 18 (1) (2019) 41–58, https://doi.org/10.1038/nrd.2018.168.

[8] B. Cvek, Nonprofit drugs as the salvation of the world's healthcare systems: the case of antabuse (disulfiram), Drug Discov. Today 17 (9–10) (2012) 409–412, https://doi.org/10.1016/j.drudis.2011.12.010.

[9] B.M. Benkő, D.A. Lamprou, A. Sebestyén, R. Zelkó, I. Sebe, Clinical, pharmacological, and formulation evaluation of disulfiram in the treatment of glioblastoma - a systematic literature review, Expert Opin. Drug Deliv. 20 (4) (2023) 541–557, https://doi.org/10.1080/17425247.2023.2190581.

[10] D. Denoyer, S. Masaldan, L. Fontaine, M.A. Cater, Targeting copper in cancer therapy: 'copper that cancer', Metallomics 7 (2015) 1459–1476, https://doi.org/10.1039/C5MT00149H.

[11] X. Lun, J.C. Wells, N. Grinshtein, J.C. King, X. Hao, N. Dang, X. Wang, A. Aman, D. Uehling, A. Datti, J.L. Wrana, J.C. Easaw, A. Luchman, S. Weiss, J.G. Cairncross, D.R. Kaplan, S.M. Robbins, Disulfiram when combined with copper enhances the therapeutic effects of temozolomide for the treatment of glioblastoma, Clin. Cancer Res. 22 (15) (2016) 3860–3875, https://doi.org/10.1158/1078-0432.CCR-15-1798.

[12] Y. Zhang, S. Ding, J. Li, X. Peng, J. Li, J. Chang, In vivo formation of cu$(DDC)_2$ complex induced by nanomedicine for mesothelioma chemotherapy, Chin. Chem. Lett. 31 (12) (2020) 3168–3172, https://doi.org/10.1016/j.cclet.2020.04.051.

[13] D. Yoshida, Y. Ikeda, S. Nakazawa, Quantitative analysis of copper, zinc and copper/zinc ratio in selected human brain tumors, J. Neuro-Oncol. 16 (2) (1993) 109–115, https://doi.org/10.1007/BF01324697.

[14] A. Gozdz, Proteasome inhibitors against glioblastoma-overview of molecular mechanisms of cytotoxicity, progress in clinical trials, and perspective for use in personalized medicine, Curr. Oncol. 30 (11) (2023) 9676–9688, https://doi.org/10.3390/curroncol30110702.

[15] P.S.O. Brien, Y. Xi, J.R. Miller, A.L. Brownell, Q. Zeng, G.H. Yoo, D.M. Garshott, M. B.O. Brien, A.E. Galinato, P. Cai, N. Narula, M.U. Callaghan, R.J. Kaufman, A. M. Fribley, Disulfiram (Antabuse) activates ROS-dependent ER stress and apoptosis in oral cavity squamous cell carcinoma, J. Clin. Med. 8 (5) (2019) 611, https://doi.org/10.3390/jcm8050611.

[16] J. Triscott, M.R. Pambid, S.E. Dunn, Concise review: Bullseye: targeting cancer stem cells to improve the treatment of gliomas by repurposing disulfiram, Stem Cells 33 (4) (2015) 1042–1106, https://doi.org/10.1002/stem.1956.

[17] C. Lu, X. Li, Y. Ren, X. Zhang, Disulfiram: a novel repurposed drug for cancer therapy, Cancer Chemother. Pharmacol. 87 (2) (2021) 159–172, https://doi.org/10.1007/s00280-020-04216-8.

[18] A. Mcmahon, W. Chen, F. Li, Old wine in new bottles: advanced drug delivery systems for disulfiram-based cancer therapy, J. Control. Release 319 (2020) 352–359, https://doi.org/10.1016/j.jconrel.2020.01.001.

[19] V. Kannappan, M. Ali, B. Small, G. Rajendran, S. Elzhenni, H. Taj, W. Wang, Q. P. Dou, Recent advances in repurposing disulfiram and disulfiram derivatives as copper-dependent anticancer agents, Front. Mol. Biosci. 8 (2021) 741316, https://doi.org/10.3389/fmolb.2021.741316.

[20] B. Xu, S. Wang, R. Li, K. Chen, L. He, M. Deng, V. Kannappan, J. Zha, H. Dong, W. Wang, Disulfiram/copper selectively eradicates AML leukemia stem cells in vitro and in vivo by simultaneous induction of ROS-JNK and inhibition of NF-κB and Nrf2, Cell Death Dis. 8 (5) (2017) e2797, https://doi.org/10.1038/CDDIS.2017.176.

[21] X. Li, F. Xu, Y. He, Y. Li, J. Hou, G. Yang, S. Zhou, A hierarchical structured ultrafine fiber device for preventing postoperative recurrence and metastasis of breast cancer, Adv. Funct. Mater. 30 (45) (2020) 2004851, https://doi.org/10.1002/adfm.202004851.
[22] J.E. Meneguello, L.S. Murase, J.V.P. de Souza, C.G. de Oliveira, L.D. Ghiraldi-Lopes, J.J.V. Teixeira, R.B.L. de Scodro, K.R.C. Ferracioli, V.L.D. Siqueira, P.A. Z. Campanerut-Sá, R.F. Cardoso, Systematic review of disulfiram as an antibacterial agent: what is the evidence? Int. J. Antimicrob. Agents 59 (5) (2022) 106578 https://doi.org/10.1016/j.ijantimicag.2022.106578.
[23] R. Thakare, M. Shukla, G. Kaul, A. Dasgupta, S. Chopra, Repurposing disulfiram for treatment of *Staphylococcus aureus* infections, Int. J. Antimicrob. Agents 53 (6) (2019) 709–715, https://doi.org/10.1016/j.ijantimicag.2019.03.024.
[24] C. Xie, J. Yan, S. Cao, R. Liu, B. Sun, Y. Xie, K. Qu, W. Zhang, Z. Weng, Z. Wang, Bi-layered disulfiram-loaded fiber membranes with antibacterial properties for wound dressing, Appl. Biochem. Biotechnol. 194 (3) (2022) 1359–1372, https://doi.org/10.1007/s12010-021-03663-0.
[25] N. Ramadhani, M. Shabir, C. McConville, Preparation and characterisation of Kolliphor®P 188 and P 237 solid dispersion oral tablets containing the poorly water-soluble drug disulfiram, Int. J. Pharm. 475 (1) (2014) 514–522, https://doi.org/10.1016/j.ijpharm.2014.09.013.
[26] G. El Fawal, M.M. Abu-Serie, H. El-Gendi, E.M. El-Fakharany, Fabrication, characterization and in vitro evaluation of disulfiram-loaded cellulose acetate/poly (ethylene oxide) nanofiber scaffold for breast and colon cancer cell lines treatment, Int. J. Biol. Macromol. 204 (2022) 555–564, https://doi.org/10.1016/j.ijbiomac.2022.01.145.
[27] P. Wang, Q. Luo, L. Zhang, X. Qu, X. Che, S. Cai, Y. Liu, A disulfiram / copper gluconate co-loaded bi-layered long-term drug delivery system for intraperitoneal treatment of peritoneal carcinomatosis, Colloids Surf. B: Biointerfaces 231 (2023) 113558, https://doi.org/10.1016/j.colsurfb.2023.113558.
[28] J. Zhao, W. Cui, Functional electrospun fibers for local therapy of cancer, Adv. Fiber Mater. 2 (2020) 229–245, https://doi.org/10.1007/s42765-020-00053-9.
[29] G. El Fawal, M.M. Abu-Serie, X. Mo, H. Wang, Diethyldithiocarbamate/silk fibroin/polyethylene oxide nanofibrous for cancer therapy: fabrication, characterization and in vitro evaluation, Int. J. Biol. Macromol. 193 (2021) 293–299, https://doi.org/10.1016/j.ijbiomac.2021.10.039.
[30] D. Han, R. Serra, N. Gorelick, U. Fatima, C.G. Eberhart, H. Brem, B. Tyler, A. J. Steckl, Multi-layered core-sheath fiber membranes for controlled drug release in the local treatment of brain tumor, Sci. Rep. 9 (2019) 17936, https://doi.org/10.1038/s41598-019-54283-y.
[31] M. Khodadadi, S. Alijani, M. Montazeri, N. Esmaeilizadeh, S.S. Younes, Recent advances in electrospun nanofiber-mediated drug delivery strategies for localized cancer chemotherapy, J. Biomed. Mater. Res. A 108 (7) (2020) 1444–1458, https://doi.org/10.1002/jbm.a.36912.
[32] R. Molina-Peña, N.H. Ferreira, C. Roy, L. Roncali, M. Najberg, S. Avril, M. Zarur, W. Bourgeois, A. Ferreirós, C. Lucchi, F. Cavallieri, F. Hindré, G. Tosi, G. Biagini, F. Valzania, F. Berger, M. Abal, A. Rousseau, F. Boury, C. Alvarez-Lorenzo, E. Garcion, Implantable SDF-1α-loaded silk fibroin hyaluronic acid aerogel sponges as an instructive component of the glioblastoma ecosystem: between chemoattraction and tumor shaping into resection cavities, Acta Biomater. 173 (2024) 261–282, https://doi.org/10.1016/j.actbio.2023.10.022.
[33] G. Sabarees, G.P. Tamilarasi, V. Velmurugan, V. Alagarsamy, B.Z. Sibuh, M. Sikarwar, P. Taneja, A. Kumar, P.K. Gupta, Emerging trends in silk fibroin-based nanofibers for impaired wound healing, J. Drug Deliv. Sci. Technol. 79 (2023) (2023) 103994, https://doi.org/10.1016/j.jddst.2022.103994.
[34] B. Kundu, R. Rajkhowa, S.C. Kundu, X. Wang, Silk fibroin biomaterials for tissue regenerations, Adv. Drug Deliv. Rev. 65 (4) (2013) 457–470, https://doi.org/10.1016/j.addr.2012.09.043.
[35] M.M. Moisenovich, E.Y. Plotnikov, A.M. Moysenovich, D.N. Silachev, T.I. Danilina, E.S. Savchenko, M.M. Bobrova, L.A. Safonova, V.V. Tatarskiy, M.S. Kotliarova, I. I. Agapov, D.B. Zorov, Effect of silk fibroin on neuroregeneration after traumatic brain injury, Neurochem. Res. 44 (10) (2019) 2261–2272, https://doi.org/10.1007/s11064-018-2691-8.
[36] Y. Qu, X. Sun, L. Ma, C. Li, Z. Xu, W. Ma, Y. Zhou, Z. Zhao, D. Ma, Therapeutic effect of disulfiram inclusion complex embedded in hydroxypropyl-β-cyclodextrin on intracranial glioma-bearing male rats via intranasal route, Eur. J. Pharm. Sci. 156 (2021) 105590, https://doi.org/10.1016/j.ejps.2020.105590.
[37] F.L. Matassoli, I.C. Leão, B.B. Bezerra, R.B. Pollard, D. Lütjohann, J.E.K. Hildreth, L.B. de Arruda, Hydroxypropyl-beta-cyclodextrin reduces inflammatory signaling from monocytes: possible implications for suppression of HIV chronic immune activation, mSphere 3 (6) (2018) 101128, https://doi.org/10.1128/msphere.00497-18.
[38] M. Malanga, J. Szemán, É. Fenyvesi, I. Puskás, K. Csabai, G. Gyémánt, F. Fenyvesi, L. Szente, "Back to the future": a new look at hydroxypropyl beta-cyclodextrins, J. Pharm. Sci. 105 (9) (2016) 2921–2931, https://doi.org/10.1016/j.xphs.2016.04.034.
[39] C. Alvarez-lorenzo, C.A. García-González, A. Concheiro, Cyclodextrins as versatile building blocks for regenerative medicine, J. Control. Release 268 (2017) 269–281, https://doi.org/10.1016/j.jconrel.2017.10.038.
[40] A. Costoya, A. Concheiro, C. Alvarez-lorenzo, Electrospun fibers of cyclodextrins and poly(cyclodextrins), Molecules 22 (2) (2017) 230, https://doi.org/10.3390/molecules22020230.
[41] I. Gonzalez-Prada, A. Borges, B. Santos-Torres, B. Magariños, M. Simões, A. Concheiro, C. Alvarez-Lorenzo, Antimicrobial cyclodextrin-assisted electrospun fibers loaded with carvacrol, citronellol and cinnamic acid for wound healing, Int. J. Biol. Macromol. 277 (2024) 134154, https://doi.org/10.1016/j.ijbiomac.2024.134154.
[42] H. Li, J. Wang, C. Wu, L. Wang, Z. Chen, The combination of disulfiram and copper for cancer treatment, Drug Discov. Today 25 (6) (2020) 1099–1108, https://doi.org/10.1016/j.drudis.2020.04.003.
[43] K. Jomova, M. Makova, S.Y. Alomar, S.H. Alwasel, E. Nepovimova, K. Kuca, C. J. Rhodes, M. Valko, Essential metals in health and disease, Chem. Biol. Interact. 367 (2022) 110173, https://doi.org/10.1016/j.cbi.2022.110173.
[44] J. Rihel, Copper on the brain, Nat. Chem. Biol. 14 (2008) 638–639, https://doi.org/10.1038/s41589-018-0089-1.
[45] L. Chen, J. Min, F. Wang, Copper homeostasis and cuproptosis in health and disease, Sig. Transduct. Target. Ther. 7 (2022) 378, https://doi.org/10.1038/s41392-022-01229-y.
[46] T. Lech, J.K. Sadlik, Copper concentration in body tissues and fluids in normal subjects of southern Poland, Biol. Trace Elem. Res. 118 (2007) 10–15, https://doi.org/10.1007/s12011-007-0014-z.
[47] I.F. Scheiber, R. Dringen, Astrocyte functions in the copper homeostasis of the brain, Neurochem. Int. 62 (2013) 556–565, https://doi.org/10.1016/j.neuint.2012.08.017.
[48] S. Jin, L. Ren, K. Yang, Bio-functional cu containing biomaterials: a new way to enhance bio-adaption of biomaterials, J. Mater. Sci. Technol. 32 (9) (2016) 835–839, https://doi.org/10.1016/j.jmst.2016.06.022.
[49] V. Oliveri, Biomedical applications of copper ionophores, Coord. Chem. Rev. 422 (2020) 213474, https://doi.org/10.1016/j.ccr.2020.213474.
[50] O.J. Moon, C.J. Yoon, J.S. Lee, H.H. Kim, Y.H. Seol, J. Lee, Tumor-specific release of copper-incorporated diethyldithiocarbamate from an optimized apoferritin scaffold enables both potent and safe anti-cancer therapy, Chem. Eng. J. 473 (2023) 145176, https://doi.org/10.1016/j.cej.2023.145176.
[51] M. Lu, A. Pais, R. Vitorino, A. Fortuna, C. Vitorino, Expediting disulfiram assays through a systematic analytical quality by design approach, Chemosensors 9 (2021) 172, https://doi.org/10.3390/chemosensors9070172.
[52] C. Leão, A. Borges, M. Simões, NSAIDs as a drug repurposing strategy for biofilm control, Antibiotics 9 (9) (2020) 591, https://doi.org/10.3390/antibiotics9090591.
[53] C. Wiegand, T. Heinze, U.C. Hipler, Comparative in vitro study on cytotoxicity, antimicrobial activity, and binding capacity for pathophysiological factors in chronic wounds of alginate and silver-containing alginate, Wound Repair Regen. 17 (4) (2009) 511–521, https://doi.org/10.1111/j.1524-475X.2009.00503.x.
[54] K.D. McCarthy, J. de Vellis, Preparation of separate astroglial and oligodendroglial cell cultures from rat cerebral tissue, J. Cell Biol. 85 (3) (1980) 890–902, https://doi.org/10.1083/jcb.85.3.890.
[55] N.A. Franken, H.M. Rodermond, J. Stap, J. Haveman, C. van Bree, Clonogenic assay of cells in vitro, Nat. Protoc. 1 (5) (2006) 2315–2319, https://doi.org/10.1038/nprot.2006.339.
[56] Kauer T., Figueiredo JL., Hingtgen S. et al. Encapsulated therapeutic stem cells implanted in the tumor resection cavity induce cell death in gliomas. Nat. Neurosci. 15 (2012) 197–204. doi:https://doi.org/10.1038/nn.3019.
[57] J. Bianco, C. Bastiancich, N. Joudiou, B. Gallez, A. Rieux, des, Danhier F., Novel model of orthotopic U-87 MG glioblastoma resection in athymic nude mice, J. Neurosci. Methods 284 (2017) 96–102, https://doi.org/10.1016/j.jneumeth.2017.04.019.
[58] H. Zhu, L. Leiss, N. Yang, C.B. Rygh, S.S. Mitra, S.H. Cheshier, I.L. Weissman, B. Huang, H. Miletic, R. Bjerkvig, P.Ø. Enger, X. Li, J. Wang, et al., Surgical debulking promotes recruitment of macrophages and triggers glioblastoma phagocytosis in combination with CD47 blocking immunotherapy, Oncotarget 8 (2017) 12145–12155, https://doi.org/10.18632/oncotarget.14553.
[59] B.M. Benkő, G. Tóth, D. Moldvai, S. Kádár, E. Szabó, Z.I. Szabó, M. Kraszni, L. Szente, B. Fiser, A. Sebestyén, R. Zelkó, I. Sebe, Cyclodextrin encapsulation enabling the anticancer repositioning of disulfiram: preparation, analytical and in vitro biological characterization of the inclusion complexes, Int. J. Pharm. 657 (2024) 124187, https://doi.org/10.1016/j.ijpharm.2024.124187.
[60] J. Hua, H. You, X. Li, R. You, L. Ma, Cu(II) ion loading in silk fibroin scaffolds with silk I structure, Int. J. Biol. Macromol. 158 (2020) 275–281, https://doi.org/10.1016/j.ijbiomac.2020.04.094.
[61] G.H. Altman, F. Diaz, C. Jakuba, T. Calabro, R.L. Horan, J. Chen, H. Lu, J. Richmond, D.L. Kaplan, Silk-based biomaterials, Biomaterials 24 (2003) 401–416, https://doi.org/10.1016/S0142-9612(02)00353-8.
[62] C.J. van Oss, M.K. Chaudhury, R.J. Good, Monopolar surfaces, Adv. Colloid Interf. Sci. 28 (C) (1987) 35–64, https://doi.org/10.1016/0001-8686(87)80008-8.
[63] S. Cai, C. Wu, W. Yang, W. Liang, H. Yu, L. Liu, Recent advance in surface modification for regulating cell adhesion and behaviors, Nanotechnol. Rev. 9 (1) (2020) 971–989, https://doi.org/10.1515/ntrev-2020-0076.
[64] P.W. Halcrow, N. Khan, G. Datta, J.E. Ohm, X. Chen, J.D. Geiger, Importance of measuring endolysosome, cytosolic, and extracellular pH in understanding the pathogenesis of and possible treatments for glioblastoma multiforme, Cancer Rep. 2 (6) (2019) 2–7, https://doi.org/10.1002/cnr2.1193.
[65] A.S. Lammel, X. Hu, S. Park, D.L. Kaplan, T.R. Scheibel, Controlling silk fibroin particle features for drug delivery, Biomaterials 31 (16) (2010) 4583–4591, https://doi.org/10.1016/j.biomaterials.2010.02.024.
[66] X. Qiao, R. Miller, Influence of pH on the surface and foaming properties of aqueous silk fibroin solutions, Soft Matter 16 (2020) 3695–3704, https://doi.org/10.1039/c9sm02372k.
[67] X. Shen, H. Sheng, Y. Zhang, X. Dong, L. Kou, Q. Yao, X. Zhao, Nanomedicine-based disulfiram and metal ion co-delivery strategies for cancer treatment, Int. J. Pharm. X 7 (2024) 100248, https://doi.org/10.1016/j.ijpx.2024.100248.
[68] M. Haeili, C. Moore, C.J.C. Davis, J.B. Cochran, S. Shah, T.B. Shrestha, Y. Zhang, S. H. Bossmann, W.H. Benjamin, O. Kutsch, F. Wolschendorf, Copper complexation screen reveals compounds with potent antibiotic properties against methicillin-

resistant *Staphylococcus aureus*, Antimicrob. Agents Chemother. 58 (2014), https://doi.org/10.1128/AAC.02316-13.

[69] P. Liu, S. Brown, T. Goktug, P. Channathodiyil, V. Kannappan, J.P. Hugnot, P. O. Guichet, X. Bian, A.L. Armesilla, J.L. Darling, W. Wang, Cytotoxic effect of disulfiram/copper on human glioblastoma cell lines and ALDH-positive cancer-stem-like cells, Br. J. Cancer 107 (9) (2012) 1488–1497, https://doi.org/10.1038/bjc.2012.442.

[70] D. Chen, Q.C. Cui, H. Yang, Q.P. Dou, Disulfiram, a clinically used anti-alcoholism drug and copper-binding agent, induces apoptotic cell death in breast cancer cultures and xenografts via inhibition of the proteasome activity, Cancer Res. 66 (21) (2006) 10425–10433, https://doi.org/10.1158/0008-5472.CAN-06-2126.

[71] M.A. Westhoff, S. Zhou, L. Nonnenmacher, G. Karpel-Massler, C. Jennewein, M. Schneider, M.E. Halatsch, N.O. Carragher, B. Baumann, A. Krause, T. Simmet, M.G. Bachem, C.R. Wirtz, K.M. Debatin, Inhibition of NF-κB signaling ablates the invasive phenotype of glioblastoma, Mol. Cancer Res. 11 (12) (2013) 1611–1623, https://doi.org/10.1158/1541-7786.MCR-13-0435-T.

[72] I.F. Scheiber, J.F. Mercer, R. Dringen, Metabolism and functions of copper in brain, Prog. Neurobiol. 116 (2014) 33–57, https://doi.org/10.1016/j.pneurobio.2014.01.002.

[73] S. Brem, S.A. Grossman, K.A. Carson, P. New, S. Phuphanich, J.B. Alavi, T. Mikkelsen, J.D. Fisher, New approaches to brain tumor therapy CNS consortium. Phase 2 trial of copper depletion and penicillamine as antiangiogenesis therapy of glioblastoma, Neuro-Oncology 7 (3) (2005) 246–253, https://doi.org/10.1215/S1152851704000869.

[74] Y. Li, S.Y. Fu, L.H. Wang, F.Y. Wang, N.N. Wang, Q. Cao, Y.T. Wang, J.Y. Yang, C. F. Wu, Copper improves the anti-angiogenic activity of disulfiram through the EGFR/Src/VEGF pathway in gliomas, Cancer Lett. 369 (1) (2015) 86–96, https://doi.org/10.1016/j.canlet.2015.07.029.